We are IntechOpen,
the world's leading publisher of
Open Access books
Built by scientists, for scientists

6,900
Open access books available

186,000
International authors and editors

200M
Downloads

Our authors are among the

154
Countries delivered to

TOP 1%
most cited scientists

12.2%
Contributors from top 500 universities

CLARIVATE ANALYTICS
BOOK CITATION INDEX
INDEXED

WEB OF SCIENCE™

Selection of our books indexed in the Book Citation Index
in Web of Science™ Core Collection (BKCI)

Interested in publishing with us?
Contact book.department@intechopen.com

Numbers displayed above are based on latest data collected.
For more information visit www.intechopen.com

Applications of In–Fiber Acousto–Optic Devices

C. Cuadrado-Laborde[1,2], A. Díez[1], M. V. Andrés[1],
J. L. Cruz[1], M. Bello-Jimenez[1], I. L. Villegas[1,3],
A. Martínez-Gámez[3] and Y. O. Barmenkov[1,3]

1. Introduction

Nowadays, in-fiber acousto-optic devices are increasingly used as frequency shifters, multiplexers, modulators, and tunable filters. They can be easily spliced into optical fiber systems, and the consequent low insertion loss, make them an attractive alternative to bulk optics devices. Our group, established at the Institute of Materials Science, Department of Applied Physics, of the Valencia University (ICMUV, Valencia, Spain), has been involved in this field for the last ten years, and our fabrication facilities allow us the development of new in-fiber acousto-optic devices for novel applications in different fields such as sensors, microwave photonics, lasers, and optical communications. Our aim here is to present the great potential shown by in-fiber acousto-optic devices for different photonic applications. Although this chapter is focused in our latest developments, the reader will also find discussed the work done by other research groups in the field. This chapter is divided in two main sections: Section 2 is focused on novel applications of acousto-optic fiber devices based on flexural acoustic waves, and Section 3 is focused on applications of the acousto-optic devices based on the interaction of longitudinal acoustic waves with fiber Bragg gratings (FBG). Finally, our conclusions are shown in Section 4.

2. Applications of acousto-optic devices based on flexural acoustic waves

In a standard single mode fiber, when a flexural acoustic wave propagates along an optical fiber a periodic perturbation is introduced in its refractive index, and it can induce coupling between the fundamental mode guided by the core and the modes supported by the cladding (Kim et al., 1997). This acousto-optic interaction can be seen as the dynamic counterpart of a long period grating (LPG). LPGs are usually fabricated by creating a periodic perturbation of the refractive index by UV radiation; this of course fixes its spectral characteristics. On the other hand, when the perturbation is introduced by an acoustic wave, its period and strength can be controlled through the frequency and amplitude of the acoustic wave, respectively. Thus, the spectral properties of the optical device can be controlled dynamically through the characteristics of the acoustic perturbation. The optical

[1]*Departamento de Física Aplicada y Electromagnetismo, ICMUV,*
Universidad de Valencia, Burjassot, Valencia, Spain
[2]*CONICET La Plata, Buenos Aires, Argentina,*
[3]*Centro de Investigaciones en Óptica, León, Guanajuato, Mexico*

coupling is resonant in wavelength; it takes place at the optical wavelength that verifies the phase-matching condition between the beat length of the two optical modes and the acoustic wavelength. At the output of the acousto-optic device, only the light that remains guided by the core mode is transmitted. Thus, the coupling of power from the fundamental mode to a cladding mode results in the appearance of an attenuation notch in the spectrum, whose amplitude is fixed when travelling acoustic waves are used. The characteristics of the fundamental flexural acoustic mode of an optical fiber fulfill the above requirements for the development of efficient in-fiber acousto-optic devices. In subsection 2.1 we will describe a Q-switched fiber laser where cavity loss modulation is reached by using this operation principle. As an interesting alternative, if standing –instead of travelling– acoustic waves are used, light transmitted at the resonance wavelength will experience an amplitude modulation at twice the frequency of the acoustic wave. In subsection 2.2 we describe a mode-locked fiber laser based on the use of this operation principle.

2.1 Q-switching by intermodal acousto-optic modulation in an optical fiber

Q-switched fiber lasers have attractive applications in different fields, such as in remote sensing and material processing. The mechanism of short pulse emission is based on the modulation of the Q factor of the cavity, which can be done either passively or actively (Siegman, 1986). In the former the setups are simpler, but the repetition rate only varies with the pump power of the medium gain. Further, they usually show long-term instability, and frequently the amplitude of the pulses is randomly modulated in time (Vicente et al., 2004). On the other hand, active Q-switching is independently and accurately controlled by an electrical signal, which triggers the modulator. The bulk approach, such as electro-optic (Kee et al, 1998) or acousto-optic modulators (Álvarez-Chávez et al., 2000), is not adapted to compact fiber laser systems required nowadays; further they have large optical coupling losses and stringent alignment requirements. For these reasons, the all-fiber approach is of permanent interest, being advantageous in terms of cost, loss, packaging, robustness, and simplicity. One solution widely investigated has been enabled by the use of FBGs as cavity mirrors. In this way, the tuning of the wavelength of one of the FBGs has been used to achieve active Q-switching (Andrés et al., 2008). Among the typical tuning methods, we could mention the stretching of fiber Bragg gratings by magnetostrictive materials (Pérez-Millán et al., 2005a; Andersen et al., 2006), by piezoelectric actuators (Imai et al., 1997; Russo et al., 2002), or by the interaction of longitudinal acoustic waves with the FBG (Delgado-Pinar et al., 2006; Cuadrado-Laborde et al., 2007). Other technique used for active Q-switching relied in the cavity loss modulation by the core-to-cladding mode-coupling in optical fibers induced by travelling flexural acoustic waves (Huang et al., 2000; Zalvidea et al., 2005). As opposed to the last two referred works –which were focused at the erbium lasing wavelength–, here we experimentally demonstrate the possibility of using this modulating technique at the technologically relevant ytterbium lasing wavelength (Tuchin, 1993). Very few actively Q-switched ytterbium-doped lasers with an all-fiber configuration have been reported (Andersen et al., 2006). The main difficulties arise from a relatively long time response and a limited modulation depth of all-fiber amplitude modulators. Here, we present the experimental results that we have obtained in a research work focused on the exploitation of in-fiber acousto-optics. In our proposed Q-switched fiber laser, when the acoustical signal is switched-off, the optical power losses within the cavity are reduced, and then a laser pulse is emitted (Villegas et al., 2011b).
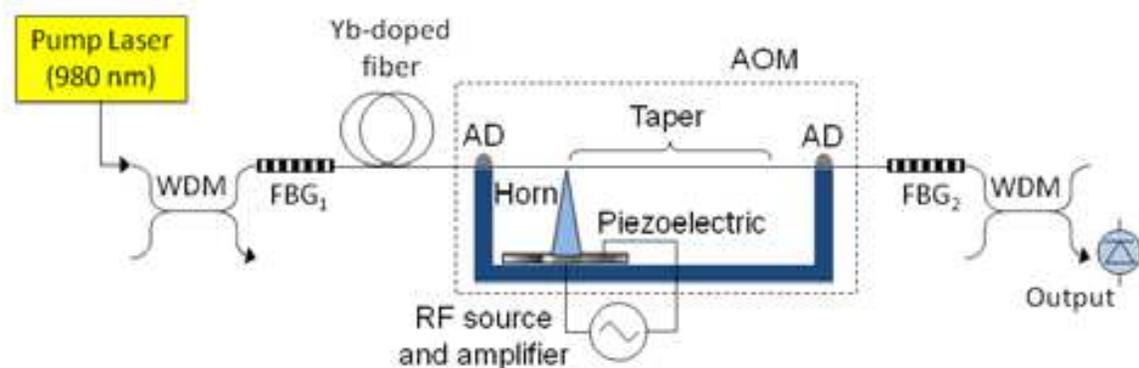
Fig. 1. *Q*-switched fiber-laser setup; the acousto-optic modulator is defined by the elements inside the dashed line; AD stands for acoustic dumper

The setup used for our *Q*-switched fiber laser is schematically illustrated in Fig. 1. The gain was provided by 0.65 m of a heavily-doped ytterbium-doped single-mode fiber –Nufern SM-YSF-HI, cut-off wavelength of 860 ± 70 nm, numerical aperture of 0.11, and fiber absorption of 250 dB/m at 975 nm–. The active fiber was pumped through a WDM coupler by a pigtailed laser diode emitting at 980 nm, providing a maximum pump power of 110 mW. The in-fiber acousto-optic modulator (AOM) was spliced between FBG_1 –Bragg wavelength at 1064 nm, FWHM of 0.23 nm, and 99.6 % of maximum reflectivity– and FBG_2 –Bragg wavelength at 1064 nm, FWHM of 70 pm, and 44 % of maximum reflectivity–, defining in this way a Fabry-Perot cavity. The AOM in turn is composed of an RF source, a transversal-mode piezoelectric disk, an aluminum horn, and a tapered single-mode optical fiber –Fibercore SM980 of low numerical aperture (0.13-0.15) –. The optical fiber was tapered down by the fusion and pulling technique using a travelling flame, which produces a taper waist with a uniform diameter of 76 µm and 0.1 m length, for this specific case. The tip of the aluminum cone –with the piezoelectric disc fixed to its base–, was glued to an uncoated section of fiber near the taper, see Fig. 1. Finally, the optical fiber in the AOM was acoustically dumped in both extremes; see Fig. 1, in order to prevent unwanted acoustical reflections.

When an RF signal is applied to the piezoelectric disc, a travelling flexural acoustic wave is launched through the taper. If the acoustic wavelength matches the beat-length between the fundamental mode guided by the core and one of the optical modes supported by the cladding, then light coupled to the later remains in the cladding downstream of the taper, being finally absorbed by the fiber coating (Birks et al., 1994). Thus, the coupling of power from the fundamental mode to a cladding mode results in the appearance of an attenuation notch in the spectrum. When the acoustic frequency is varied, the periodicity of the perturbation also does, and hence the phase-matching condition is shifted to a different optical wavelength. Figure 2(a) shows the tunability of the notches caused by the coupling between the fundamental core mode and the first three cladding modes LP_{1m}. The selected operating point was at an optical wavelength of 1064.1 nm for an RF signal applied to the piezoelectric of 825 kHz. These measurements were made by illuminating the taper with a broadband light source and detecting the light transmitted through the taper with an optical spectrum analyzer. As an example, Fig. 2(b) shows one the measured transmission spectra for an applied voltage to the piezoelectric of 26 V and a frequency of 885 kHz. The transfer of optical power from the fundamental core mode to one of the cladding modes

behaves periodically as a function of the acoustic power, which in turn is a function of the applied voltage to the piezoelectric. Figure 2(c) shows this effect for the selected operation point marked in Fig. 2(a). As it can be observed, the transmittance decays by a maximum of 12 dB for an applied voltage to the piezoelectric of 50 V (peak-to-peak measurement). Beyond this point, further increment in the applied voltage raises the transmittance again. Therefore, and bearing in mind its use as a Q-switching device, cavity loss modulation between 0 dB and 12 dB can be achieved by applying to the piezoelectric a sinusoidal signal at the frequency of 825 kHz fully-modulated by a rectangular signal, see the inset of Fig. 2(c). This modulation produces on–off periods of the acoustic wave travelling down the fiber, which results in a modulation of the cavity losses at the resonance wavelength. In passing, we should mention that several tapers were fabricated in order to better optimize this laser system, by using Fibercore SM980 of high numerical aperture (0.17-0.19), and Nufern SM-YSF-LO (a moderately ytterbium-doped fiber), and in turn with different taper waists. Despite this, the minimal decay in transmittance was always around the reported values, i.e. between 10 and 16 dB.
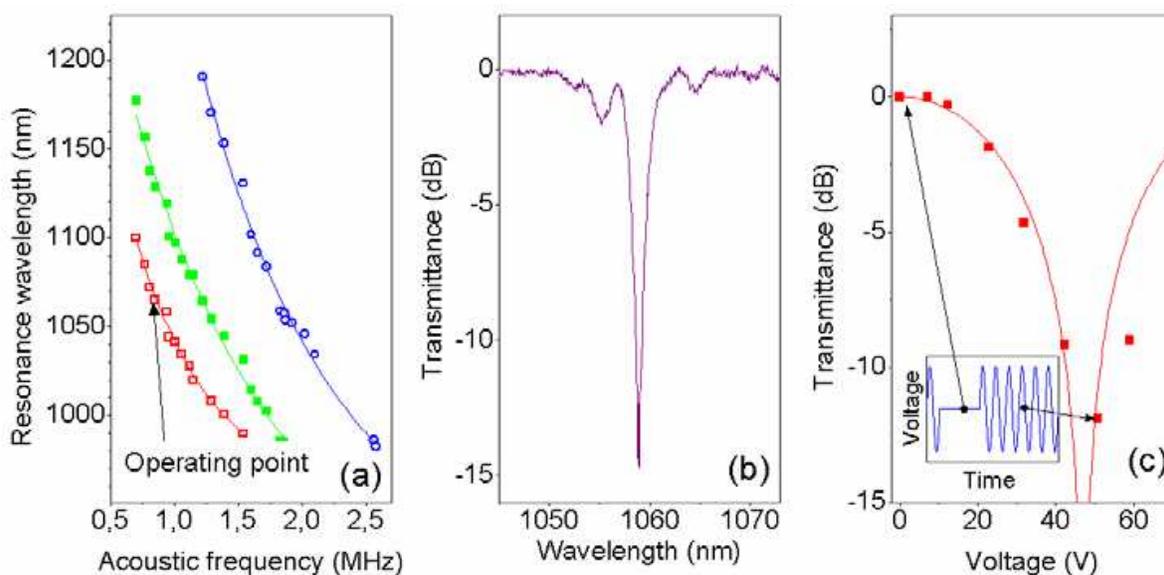

Fig. 2. (a) Resonant optical wavelengths as a function of the acoustic frequency for the first three mode-couplings LP_{01} -LP_{1m}. (b) Typical transmission notch caused by the first mode-coupling by applying to the piezoelectric a sinusoidal signal at 885 kHz and 26 V. (c) Transmittance at the selected operation point marked in (a) –i.e. 1064.1 nm and 825 kHz– as a function of the applied voltage to the piezoelectric (solid scatter points), the curve represents a theoretical fitting according to a $\sin^2$ function

The switching time is one of the key parameters for any modulator intended to be used as a Q-switching device in a fiber laser. Preferably, it should be as short as possible. For this reason we measured the temporal response of this device, by detecting the transmitted light, while simultaneously registering the modulating signal in an oscilloscope. It takes 25 μs to increase/decrease the transmitted optical power through the taper when the voltage applied to the piezoelectric is switched-off/on, respectively. This time corresponds reasonably well with the time it takes a flexural acoustical wave to travel down the taper, i.e. 0.1 m / 3764 m/s ≈ 26 μs. This value is short enough to allow the use of this modulator as a Q-switching device in a fiber laser, as it will be demonstrated in the following section. In principle, and for a

given taper waist, shorter switching times could be achieved by decreasing the interaction length. Unfortunately, this simultaneously increases the acoustical power needed to reach the same optical coupling power, therefore there is a trade-off between both parameters.
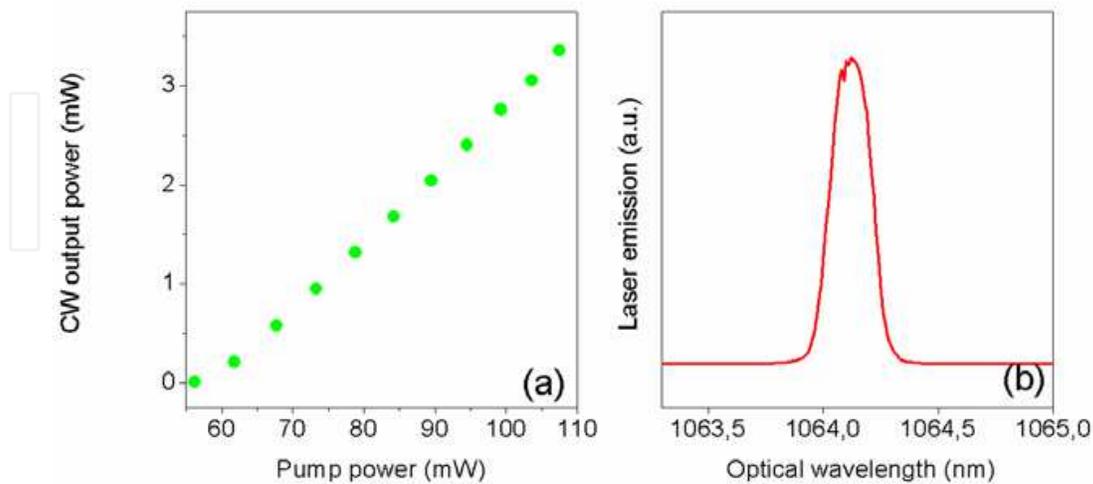

Fig. 3. (a) Output optical power in CW emission as a function of the pump power. (b) Emission spectrum

In this setup, both gratings are permanently tuned to the same wavelength by using two translational stages, one for each FBG; see the setup in Fig. 1. In this way, for zero voltage applied to the piezoelectric, this laser emits in CW, since then the cavity losses are minimal, see the transmittance in Fig. 2(c) for 0 V. Figure 3(a) shows the optical power in CW emission as a function of the pump power. There is a pump power threshold of 56 mW, about which the laser starts to emit, reaching a maximum output power of 3.4 mW, which in turn is determined by the maximum pump power available in our setup (110 mW). Figure 3(b) shows the spectrum of CW emission; its linewidth is of 0.21 nm at a center optical wavelength of 1064.1 nm.

Now, we discuss the Q-switched operation of this laser. To this end, we modulated the cavity losses by applying to the piezoelectric a fully-modulated sinusoidal signal at the frequency of 825 kHz and 50 V. A rectangular wave was used to modulate the RF voltage that generates the acoustic wave. At a given frequency of the modulating signal, we found always a maximal duty cycle –i.e. the fraction of time that the signal is in its high level– able to perform Q-switch correctly. If we decrease this duty cycle, then the cavity would stay in its high Q state longer, and more than one Q-switched pulse would be emitted in each time slot. The Q-switch repetition rate becomes determined by the frequency of the modulating signal; with this configuration we reached continuous tuning of the Q-switch repetition rate in the range 1-10 kHz. Figure 4(a) shows, as an example, a Q-switched optical pulses train at 1 kHz, together with the corresponding modulating signal, for a pump power of 59 mW. Figure 4(b) shows a detail of a single Q-switched optical pulse of the train shown in Fig. 4(a) with a time width (FWHM) of 3.72 μs. The pulses have a quasi-Gaussian profile; the fitting by this function is also shown in Fig. 4(b). The effect of pump power on the Q-switched pulses, for different repetition rates in the range 1-10 kHz, is shown in Fig. 5. For each Q-switching frequency there is a pump power threshold. Above threshold, the peak power increases with pump power, and there is a corresponding reduction of pulse width. For a given frequency there is also a pump power level beyond which extra pulses appear, the curves are truncated at that point. In order to

overtake this limitation, a modulator with improved modulation depth is required. In addition, our laser produces easily multiple pulse emission, which is a well-known problem in actively Q-switched lasers with relatively large time responses. A large time response makes critical the adjustment of the duty cycle of the modulation voltage when the pump power is increased, particularly at low repetition rates. Consequently, a faster switching response of the acousto-optic modulator is required in order to improve the operation of the laser.
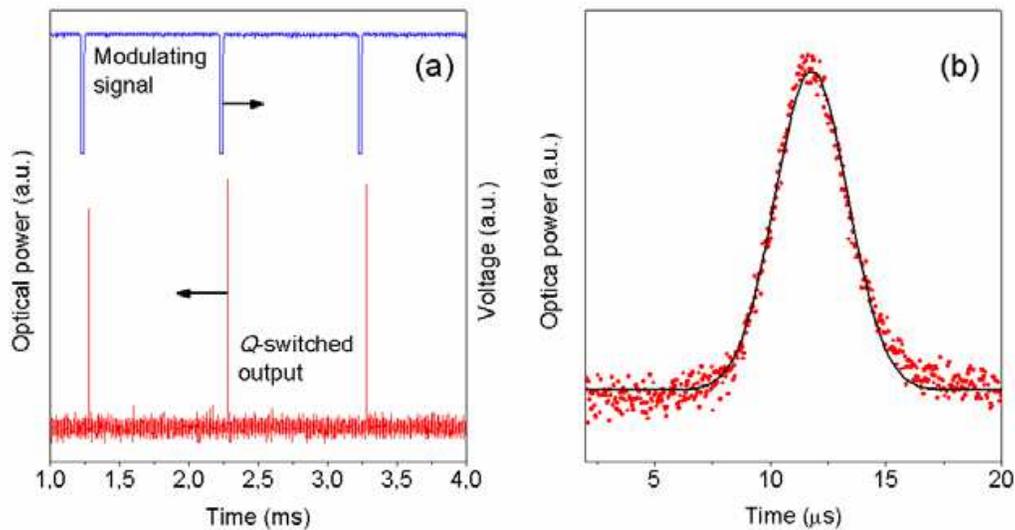

Fig. 4. (a) Modulating signal (above) at 1 kHz repetition rate together with the generated Q-switched laser output (below). (b) Detail of a single Q-switched pulse of (a) (scatter points) together with its corresponding fitting by a Gaussian function (solid curve)
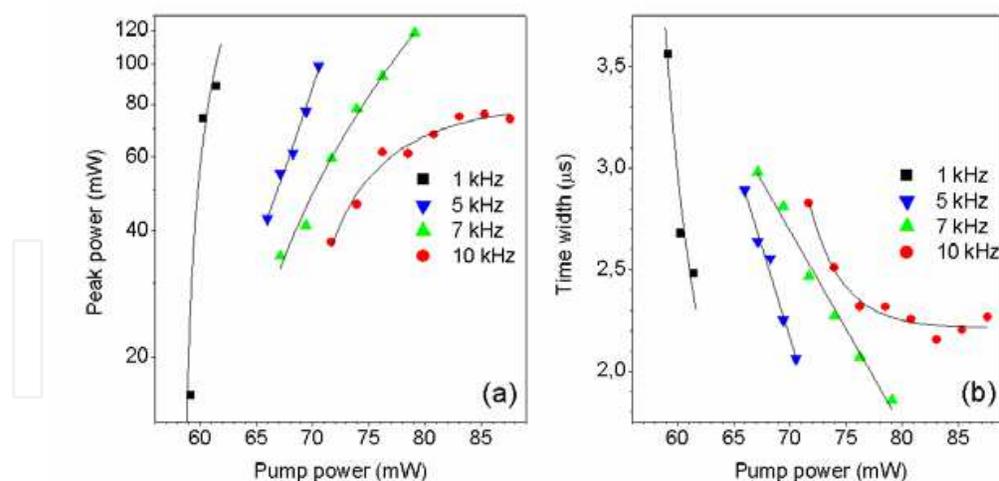

Fig. 5. Peak power and time width in Q-switched operation as a function of the pump power, (a) and (b), respectively, for several repetition rates

2.2 Mode-locking by intermodal acousto-optic modulation in an optical fiber

Mode-locking lasers have a vast number of applications, ranging from the telecommunications industry to medical surgery (Bonadeo et al., 2000; Haus, 2000; Yu et al., 2000; Schaffer et al., 2003). The shortest pulses are obtained by passive schemes. However, they also have some drawbacks, among them, they are generally unstable, they have higher

timing-jitter between pulses and usually self-starting cannot be assured. An alternative to using passive schemes that reduces jitter and allows for synchronization is to use an active scheme. To this end, a modulator is driven at the cavity's fundamental repetition rate; therefore, timing-jitter is reduced since each pulse is triggered by the modulator, which in turn is accurately driven by an electrical signal. In this way, in active mode-locking one has the possibility to synchronize a laser to an external clock or electronic signal (French, 1995). Among all these lasers, the all-fiber solution has been the subject of intensive research due to their compact structure, free alignment problems, and low cost, between other merits. Earlier and subsequent active modelocked fiber lasers were not strictly all-fiber lasers, since they currently included a bulk modulator (Geister & Ulrich, 1988; Phillips et al., 1989a; Hudson et al., 2005). This not only induces extra losses into the laser cavity but of course also destroys the benefits of an all-fiber configuration. On the contrary a strictly all-fiber modulator can overcome these limitations and it can be used for actively mode-lock rare-earth-doped silica fiber lasers (Phillips et al., 1989b; Culverhouse et al., 1995; Jeon et al., 1998; Costantini et al., 2000; Myrén & Margulis, 2005; Cuadrado-Laborde et al., 2009a, 2010a, 2010b; Bello-Jiménez et al., 2010, 2011). Table 1 shows the major achievements towards the obtaining of all-fiber actively mode-locked lasers. As it can be observed, acousto-optic devices have been by far the preferred technique, with exception of the Myrén and Marguli`s work relying in a electro-optic effect. Our group was involved in works described in the last two rows of this table, which will be discussed in detail in this chapter.

In Jeon`s et al. work (1998), mode-locking is achieved by frequency shifting based on travelling flexural acoustic waves in a two-mode optical fiber; such a frequency shifter could be considered an improved version of the one reported in (Kim et al., 1986). Unlike Jeon (1998) and Kim (1986), here we propose using a standard single-mode optical fiber in which core-to-cladding mode-coupling is induced by a standing flexural acoustic wave. In this way, the device does not work as a frequency shifter, but as an amplitude modulator, which is used to actively mode-lock a fiber laser. In the following, we demonstrate that this simple acousto-optic modulator proves to be particularly well-suited for active mode-locking purposes (Bello-Jiménez et al., 2010, 2011).

The setup of the actively modelocked fiber ring laser is schematically illustrated in Fig. 6. The medium gain was provided by 4.36 m of erbium-doped fiber (EDF) containing 300 ppm Er^{3+}, with a cut-off wavelength of 939 nm, and a numerical aperture of 0.24. The active fiber was pumped through a WDM by a 980 nm pigtailed laser diode, providing a maximum pump power of 600 mW. Next –and following a clockwise direction– it was inserted the acousto-optic modulator between two polarization controllers (PCs), followed by a delay line fusion-spliced to port one of a polarization-independent three-port optical circulator (OC). The OC not only forces the unidirectional operation within the ring but simultaneously incorporates the FBG filtering in the cavity by the second port. Finally, the ring cavity is closed by connecting port three of the OC to the WDM. The output of this laser is obtained by transmission through the FBG –Bragg wavelength at 1549.5 nm, FWHM of 0.45 nm, and 50 % of maximum reflectivity–. In this way, the entire laser is spliced. The AOM in turn is composed of an RF source, a piezoelectric disk, an aluminum conical horn, and a 0.2 m long standard optical fiber stripped of its polymer coating; in order to prevent the attenuation of the acoustic wave. The horn is attached to the piezoelectric, and it focuses the vibrations into the fiber through its tip, which is glued to the uncoated fiber. In order to allow the generations of a standing flexural acoustic wave, the uncoated optical fiber of the AOM was firmly clamped at one extreme, whereas in the other it was damped, see Fig. 6.

Year	Group	Mode-locking mechanism	Major achievements
1989	Phillips et al.	Acousto-optically induced intra-fiber phase modulation	First all-fiber actively mode-locked laser, 200 ps time width pulses
1995	Culverhouse et al.	Acousto-optically induced frequency shifting in an all-fiber four-port null coupler	18 ps time width pulses (chirped)
1998	Jeon et al.	Acousto-optically induced mode-coupling in a two-mode optical fiber	Harmonic mode-locking, 3.8 ps time width pulses
2000	Costantini et al.	Acousto-optically induced intra-fiber phase modulation	Visible up-conversion laser, 550 ps time width pulses
2005	Myrén and Margulis	Electro-optic effect in an all-fiber Mach–Zehnder interferometer	1 ns time width pulses
2009	Cuadrado-Laborde et al.	Acousto-optic super-lattice effect in a fiber Bragg grating	630 ps un-chirped time width pulses. First to demonstrate double-active all-fiber Q-switching and mode-locking
2010	Bello-Jiménez et al.	Acousto-optically induced mode-coupling in a single-mode optical fiber	34 ps time width pulses

Table 1. Major achievements in the development of all-fiber actively mode-locked lasers

Fig. 6. Modelocked fiber-laser setup; where OC stands for optical circulator, EDF for erbium doped fiber, PC for polarization controller, FBG for fiber Bragg grating, and WDM for wavelength division multiplexer. The acousto-optic modulator is defined by the elements inside the dashed line

Figure 7(a) shows the modulation depth as a function of light wavelength for an acoustic frequency of 2.37315 MHz. The voltage applied to the piezoelectric was 18 V (whenever we refer to voltages, it is a peak-to-peak measurement). The measurement was performed by

illuminating the AOM with a tunable laser and detecting the transmitted light at each wavelength. The modulation is maximal at the phase-matching wavelength of 1551 nm, and symmetrically decreases for longer and shorter wavelengths. It should be emphasized the high modulation depth achieved in this technique, reaching a maximum of 72 %, together with the relatively broad operative bandwidth of 1.5 nm (FWHM) –i.e. 187 GHz at the operation wavelength–. Moreover, the insertion loss is as low as 0.7 dB, corresponding to the maximum transmittance value attained, which is 86 %. When the acoustic frequency is varied, the periodicity of the perturbation also does, and hence the phase-matching condition is shifted to a different wavelength. Figure 7(b) illustrates this effect; the rate of change for the wavelength shift is of −0.169 nm/kHz; the maximum modulation reached at each specific operation point is also shown to the right. The differences between the modulation depths at different acoustic frequencies are mainly originated from the combination of the non-flat frequency response of the piezoelectric and the acoustic fiber resonator.
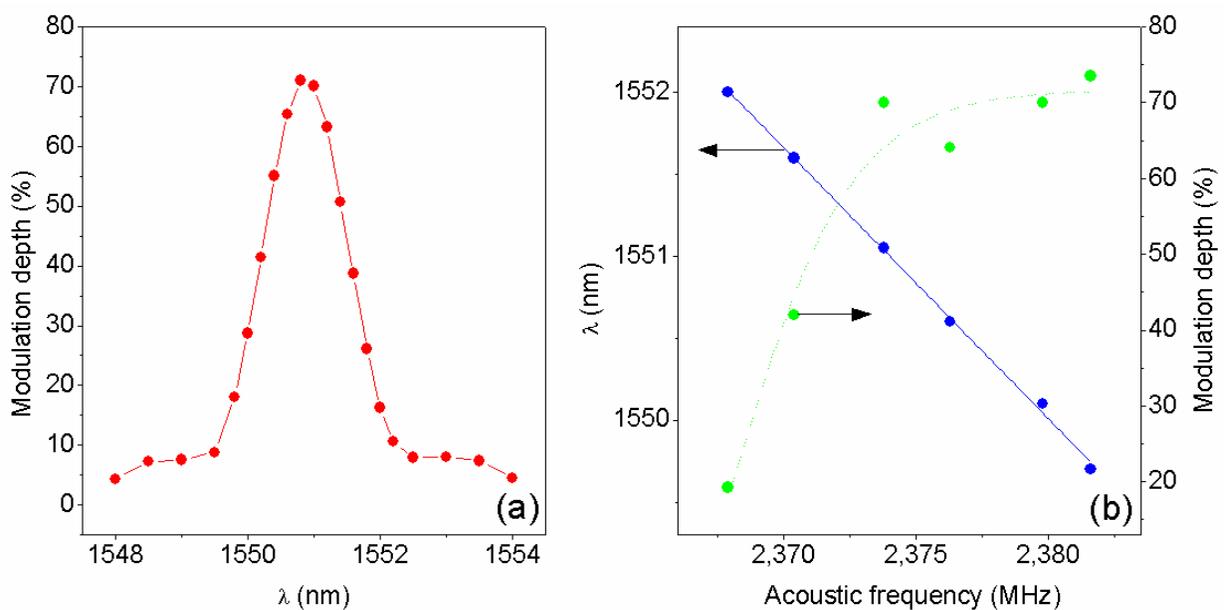
Fig. 7. (a) Modulation depth as a function of the optical wavelength for an RF signal applied to the piezoelectric of 2.37315 MHz and 18 V. (b) Resonant optical wavelengths as a function of the frequency of the RF signal, its corresponding modulation depth is also shown to the right ordinate

Now we discuss the operation of the modelocked laser shown in Fig. 6. The delay line length must be selected to match the round-trip time with the reciprocal of the optical modulation frequency, which in turn is twice the electrical frequency applied to the piezoelectric. The selected operation point for the piezoelectric is the same as in Fig. 7(a), i.e. 2.37315 MHz, and then the cavity length results in 43.7 m. However, fine tuning is always necessary to match the frequency of the modulation signal to the inverse of the round-trip time of the cavity. A translation stage was also used for matching the reflection band of the FBG to the operative wavelength (1551 nm). Regarding the dispersion of this laser; we measured the dispersion of each fiber and component within the cavity by the frequency-domain modulated-carrier method. The laser cavity is a mixed-dispersion fiber ring with an average cavity dispersion of −1 ps/nm/km (Bello-Jímenez et al., 2010). We measured also both the dispersion of the OC and WDM, both resulted normal also with a group delay per

wavelength unit of −0.3 ps/nm and −0.04 ps/nm, respectively. In this way, we can assure that this laser works under the normal dispersion regime. Figure 8(a) shows the RF signal used to drive the piezoelectric together with the modelocked train of pulses generated (50 GHz bandwidth oscilloscope). As it can be observed, the frequency of the optical train (4.756 MHz) is twice the frequency of the signal used to drive the piezoelectric (2.37315 MHz). The optical pulses were best fitted by a sech² function; neither Gaussian nor Lorentzian functions improved the fitting. This is an expected profile for the optical pulses in this type of dispersion-mixed cavities, in which both kind of dispersion coexist, i.e. normal and anomalous (Bélanger, 2005). On the other hand, according to active mode-locking theory, the time width τ of the optical pulse can be expressed as (Kuizenga & Siegman, 1970):

$$\tau = \frac{\sqrt{\sqrt{2}\ln 2}}{\pi} \sqrt[4]{\frac{g_0}{\delta_m}} \frac{1}{\sqrt{f_m \Delta f_m}}, \tag{1}$$

where f_m is the modulation frequency, g_0 is the gain of the active medium, Δf_m is the modulator bandwidth, and δ_m is the modulation depth. As a rough estimation, let us compare these results with the results reported in Cuadrado-Laborde et al. (2009a), where optical pulses of 780 ps were obtained by using also AM mode-locking, but with a different modulator and setup. Thus, by comparing them, here there is a higher modulation depth (×7), modulation bandwidth (×240), and gain (×3), but a lower modulation frequency (×0.5) –where the additional assumption that gain scales with the EDF length was made–. Therefore, there is a narrowing factor for the time width of $(3/7)^{1/4} \times (0.5 \times 240)^{-1/2} = 7.4 \times 10^{-2}$. In this way, comparatively, it should be possible to reach optical pulses around $7.4 \times 10^{-2} \times 780$ ps ≈ 58 ps in this laser, which could be taken roughly as a lower limit for this configuration. One key element, out of the preceding discussion, is the FBG bandwidth, which acts as a filter –see the setup in Fig. 6 –whose bandwidth must be selected narrower than the AOM bandwidth; otherwise modes not amplitude modulated would interfere in the mode-locking process. This evidently limits the effective bandwidth and raises the minimum pulse width able to be reached with this configuration, since modulator bandwidth and time width are inversely related. The optical pulse's peak power and temporal width as a function of the pump power are shown in Fig. 8(b). The time width as well as the peak power monotonically increases with the pump power; at the lowest pump powers, pulses as narrow as 95 ps were obtained with a pump power of 110 mW; see the inset of Fig. 8(b). Pump powers below 110 mW precludes mode-locking; whereas the upper limit is reached by the maximum pump power available in our setup.

Next, we analyzed the dependence of the pulse´s parameters with the applied voltage to the piezoelectric, see Fig. 9(a). Both the transmittance and modulation depth are functions of the applied voltage to the piezoelectric through a periodic relationship. However, we can consider that the relationship is linear within the range of voltages of Fig. 9(a). When the voltage increases, the modulation also does, and pulses become narrower, as expected from AM mode-locking theory, see Eq. (1). Finally, it is of practical interest to quantify the maximum allowable detuning ($\Delta \nu_{max}$), i.e. the maximum difference between the reciprocal of the cavity round trip´s time and modulation frequency that sustain mode-locking. Figure 9(b) shows the variation of the pulse´s parameters under frequency detuning, resulting in $\Delta \nu_{max}$ = ± 300 Hz at half the maximum peak power. According to theory of detuning in AM mode-locking (Li et al., 2001), the maximum allowable detuning can be expressed as:

$$\Delta v_{\max} = \frac{c\sqrt{m}}{4n\Delta f_m L},$$ (2)

with c the speed of light in vacuum, L is the cavity length, and n the modal effective index. Thus, the minimum locking range is attained when the whole modulation bandwidth is available, by replacing we obtain Δv_{max} = 42 Hz. This value represents a lower limit in this setup, since we are not using the whole modulator bandwidth –due to the reflection bandwidth of the FBG–. Thus, a higher measured locking range is an expected result.
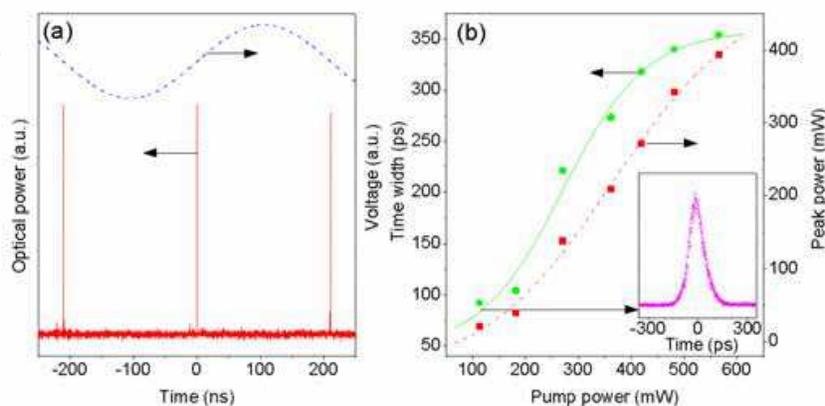

Fig. 8. (a) Voltage signal used to drive the piezoelectric and mode-locked train of pulses generated at 4.75 MHz repetition rate with 271 mW of pump power (dashed and solid curves, respectively). (b) Time width (FWHM) and peak power of the optical pulses as a function of the pump power (solid and open scatter points, respectively). The inset shows a single pulse of 95 ps time width
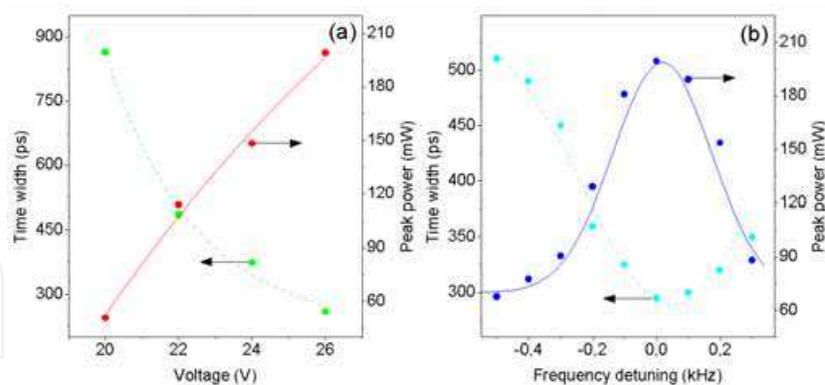
Fig. 9. (a) Time width (FWHM) and peak power as a function of the applied voltage; for a fixed frequency of 2.3731 MHz (open and solid scatter points, respectively). (b) Same as before, but as a function of the frequency detuning, for a fixed voltage of 26 V. In both cases, a pump power of 350 mW was used

Next, we carried out an experimental study of this actively mode-locked all-fiber ring laser, looking towards an improvement in its performance. To this end, we slightly modified the setup shown in Fig. 6, by replacing the FBG used before with a near 100 % reflective FBG, with a FWHM bandwidth of 0.3 nm, which should be compared with the preceding FBG with FWHM of 0.45 nm, and 50 % of maximum reflectivity. Together with this, the EDF

length was shortened up to 2.85 m. As a result of these changes, output light pulses were obtained by one of the ports of a 3 dB coupler incorporated within the ring (Bello-Jímenez et al., 2011). With this new configuration, output light pulses were obtained with a maximum peak power of 380 mW and pulse width of 90 ps. By comparing the narrowest pulses obtained with this configuration with the narrowest pulses reported before (95 ps) where the same type of AOM was used, we find nearly no difference. However, from the laser operation point of view, there is an important improvement, since the present arrangement is rather more stable, and the laser can be adjusted more easily. We attribute this improvement to the FBG used, which has a flat spectral reflectivity, making less critical the spectral matching between the FBG reflectivity with the resonant dip of the AOM. On the contrary, the FBG used before, was of nearly the same FWHM but with a lower reflectivity (50 %). As a consequence, any spectral detuning resulted in a larger variation in reflectivity, which in turn induced a higher difficulty to stabilize the laser operation. Next, we analyzed the change in the pulse`s parameters as the EDF length was varied, see Fig. 10 (a). Changes in the EDF length induced a slight shortening in the output light pulses, which is in accordance with Eq. 1, if we assume that gain scales with the EDF length. By this trend, the shortest light pulses (65 ps) were obtained at 2.2 m of EDF length. Further narrowing by this trend was not possible, since no mode-locked output pulses were observed for EDF lengths shorter than 2.15 m.
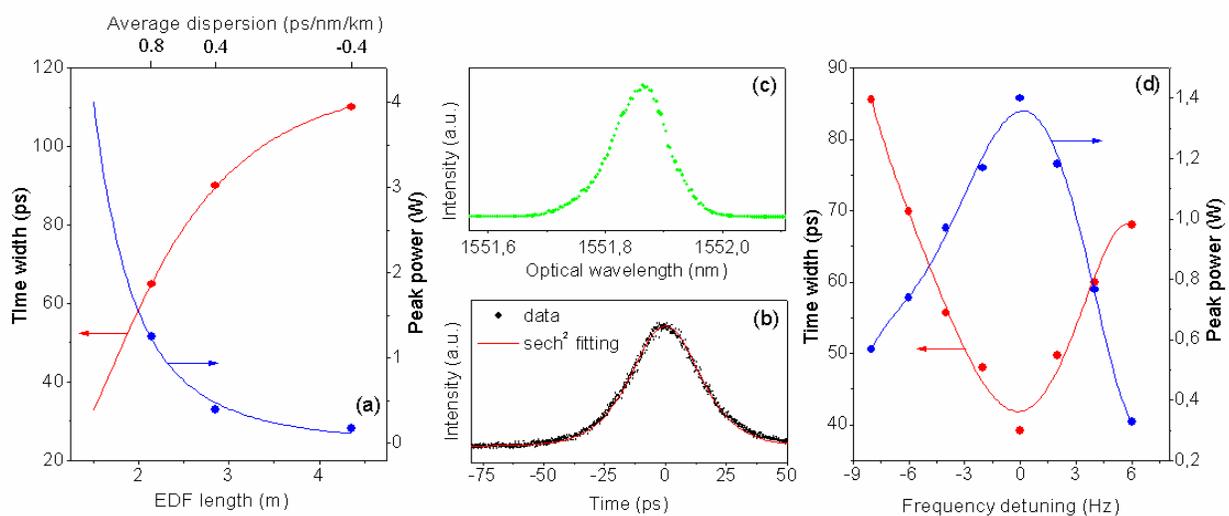
Fig. 10. (a) Time width (FWHM) and peak power as a function of the EDF length, using a FBG with 0.3 nm bandwidth. Using a 0.7 nm bandwidth: (b) single mode-locked pulse at 4.73 MHz repetition frequency, together with its corresponding fitting by a sech² function; (c) optical spectrum of the laser; (d) time width and peak power versus the frequency detuning

An important parameter of our laser arrangement is the FBG bandwidth, which acts as a spectral filter. Its bandwidth has to be selected narrower than the AOM bandwidth; in order to insure that the modes are properly amplitude modulated. For this reason we used first a 0.3 nm bandwidth FBG, which fulfills this requirement, since the AOM bandwidth is of 1.5 nm. However, it can be easily understood that a larger number of modes locked –i.e. amplitude modulated– produce the narrowest mode-locked train of pulses, which is in accordance with Eq. 1. In this respect, there is margin for improvement, since the bandwidth of the FBG used is far to be close to the AOM bandwidth. For this reason we replace the flat-top FBG with another FBG, which also has a flat-unit reflectivity, but a broader optical

bandwidth of 0.7 nm. Fig. 10(b) shows the shortest pulse obtained with this configuration, by using an EDF length of 2.45 m at a pump power of 265 mW. The measured temporal width was 34 ps (FWHM), with a maximum peak power of 1.4 W. For this pulse the spectral linewidth was measured to be 110 pm (i.e. 13.7 Ghz at 1551.9 nm), using a 50 pm resolution optical spectrum analyzer, see Fig. 10(c). On the other hand, a Fourier-transform limited sech² pulse should have a spectral linewidth of 9.3 GHz. From the comparison between this last value and the linewidth measurement, we conclude that the optical pulses of our mode-locked laser could have some moderate degree of chirp. Finally, we present the variation of the pulse parameters as a function of the frequency detuning for this configuration, see Fig. 10(d); the measured allowable frequency detuning was of 8 Hz. According to theory of detuning in AM mode locking, the maximum allowable detuning is inversely proportional to the modulator optical bandwidth, in this case replaced by the FBG bandwidth, see Eq. 2. Since the later has been increased noticeably, i.e. from 0.3 nm to 0.7 nm, a reduction in the allowable detuning is an expected result.

3. Applications of acousto-optic devices based on the interaction of longitudinal acoustic waves with fiber Bragg gratings

When a travelling axially-propagating longitudinal acoustic wave is launched through a FBG, the periodic strain field of the acoustic wave perturbs the grating in two different ways. First, the average index changes in response to the stress-optical effect and second, the otherwise uniform Bragg grating pitch changes being modulated by the acoustical signal (Russell & Liu, 2000). As a consequence of both effects the reflectivity changes, the main features of these changes depend on the ratio between the acoustical wavelength and the grating length (Andrés et al., 2008). Thus, we can distinguish two well-different situations: the long-wavelength and the short-wavelength regimes. In the first, the Bragg grating pitch is homogeneously perturbed along its length. The successive cycles of compression and expansion generated by the longitudinal wave will shift periodically in time the spectral response of the grating as a whole to longer and shorter wavelengths (Cuadrado-Laborde et al., 2007; Andrés et al., 2008). On the contrary, in the short-wavelength regime the acoustic wave generates many compressed and expanded sections, which gives rise to a superstructure within the grating. In this case, the spectral response of the original FBG shows new and narrow reflection bands symmetrically at both sides of the original Bragg wavelength (Liu et al., 1997, 1998). The position and strength of these sidebands can be controlled by varying the frequency and voltage applied to the piezoelectric, respectively. Subsections 3.1 and 3.2 show the use of these effects to modulate the *Q*-factor of a fiber laser and as an active mode-locker; i.e. long and short-wavelength regimes, respectively. Subsection 3.3 shows the use of the acousto-optic interaction in a FBG in the short-wavelength regime as a tunable photonic true-time-delay line based on the group delay change of the light reflected from the grating sidebands. Finally, when the acoustic perturbation is not a harmonic wave but a single pulse, its passage through the grating creates a defect in the FBG, which can be used to actively *Q*-switch a distributed feedback fiber laser, which is discussed in subsection 3.4.

3.1 *Q*-switching of an all-fiber laser by acousto-optic interaction in a fiber Bragg grating in the long-wavelength regime
As an example of the use of the long-wavelength regime in FBGs, we present an all-fiber acousto-optic modulator suitable for *Q*-switching applications (Cuadrado-Laborde et al.,

2007). It consists of a short-length fiber Bragg grating modulated by a standing longitudinal acoustic wave, whose wavelength is much longer than the grating length. Periodic stretching and compression of the grating due to the elastic wave, causes that the Bragg wavelength is harmonically, continuously and repeatedly tuned in time over a given wavelength range. Figure 11 illustrates the operation principle. In the long-wavelength regime, the acoustic wavelength is much larger than the grating length.

However, the amplitude of the acoustic waves that can be achieved in a realistic arrangement is rather small to produce a significant perturbation of the FBG. We found that this limitation could be overcome by using an acoustic cavity. Thereby, if the grating is placed in the proper position within the acoustic cavity, a low-frequency standing longitudinal elastic wave will produce periodic stretching and compression of the grating. As a consequence, the reflection band will shift periodically in wavelength around the original Bragg wavelength, sweeping a given wavelength range in a harmonic way. The elastic wave may also introduce some chirp in the grating due to non-uniformity of the strain induced along the grating. To achieve efficient modulations this effect must be minimized. Thus, the grating length must be short compared with the acoustic wavelength, and the positioning of the grating within the cavity must match an anti-node of the standing acoustic wave.
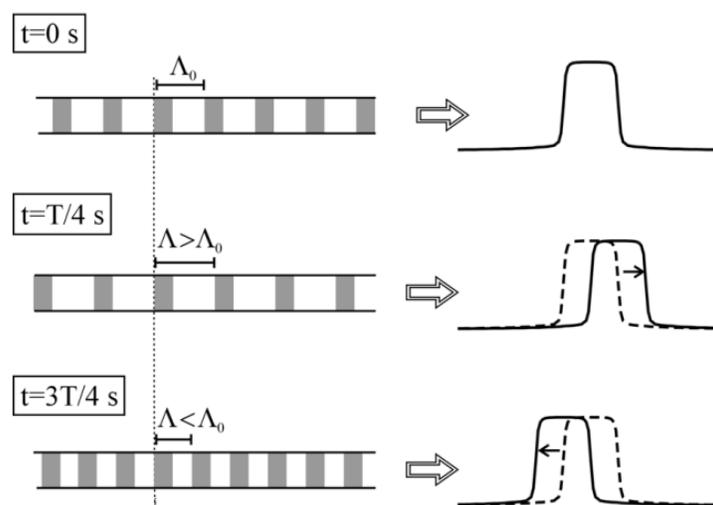
Fig. 11. Interaction of acoustic waves in the long-wavelength regime and FBGs; T is the period of the acoustic wave, Λ is the instantaneous pitch of the Bragg grating, and Λ_0 is the pitch of the Bragg grating in absence of acoustic wave. The effect on the reflection band is shown qualitatively. The standing acoustic wave stretches and compresses the grating periodically. During the time that the grating is stretched, the reflection band of the grating shifts towards longer wavelengths, whereas it shifts towards shorter wavelengths when it is compressed

Figure 12(a) shows a diagram of the laser setup, together with a detail of the acousto-optic modulator. The Fabry-Perot cavity becomes defined by FBG_1 (which also acts as modulator) and FBG_2. A piezoelectric disk (15 mm in diameter and 2 mm thickness) was used to generate the longitudinal acoustic waves, which were launched to FBG_1 through a silica horn. The base of the horn was glued to the piezoelectric and the tip reduced to ~125 μm and then fusion-spliced to FBG_1. At a distance of 210 mm from the piezoelectric disk, the fiber was clamped allowing standing acoustic waves to be created in the fiber section between the horn and the clamp. FBG_1 was written in the core of a photosensitive fiber by

UV irradiation using a phase-mask technique. The photosensitive fiber was previously tapered to enhance the acousto-optic interaction; the taper waist was 50 mm long, 90 μm in diameter, and the transition lengths were 13 mm. The grating was recorded in the taper waist (uniform diameter section); the FBG$_1$ length was 22 mm. The highest frequency used in our experiments was 61 kHz, and according to the velocity of sound in silica fibers for longitudinal elastic waves (5760 m/s), the wavelength for this frequency is 94 mm. Thus, we can verify that FBG$_1$ length is short enough to guaranty a standard long-wavelength regime. An apodization profile was introduced also during the grating inscription to reduce side-lobes in the spectrum. Figure 12(b) shows the transmission spectrum for both FBGs, the bandwidth of FBG$_1$ was 0.15 nm and the reflectivity was higher than 99.9%. On the short-wavelength side, the transmission drops sharply (~ 0.72 dB/pm). The side-lobes have been reduced entirely on this side, while a significant side-lobe still remains on the long-wavelength side of the transmission band. On the other hand, FBG$_2$ acted as the output coupler, its Bragg wavelength was 1543.27 nm, the reflectivity 50%, and the bandwidth was 40 pm.
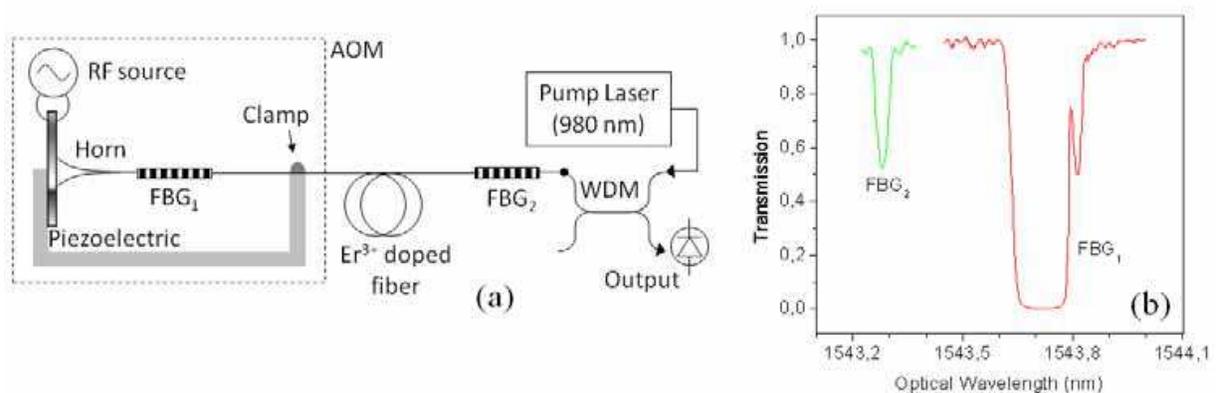
Fig. 12. (a) Laser setup, the dashed line defines the acousto-optic modulator. (b) Transmission spectra of the two fiber Bragg gratings

Next, we discuss the modulator´s performance. We detect the intensity of the light reflected by the mid-reflection point of the short-wavelength band-edge, when an AC electric signal of a given frequency was applied to the piezoelectric. To this end a tunable laser diode was used. The modulation of the grating caused by the elastic wave generates periodic modulation of the light intensity reflected by the grating. An example is shown in Fig. 13(a). At low voltage, a sinusoidal modulation was observed since the grating shifts little and the laser reflects at the band-edge at any time during the period of the electric signal. As the electric signal amplitude increases, the grating shifts further and then, the laser reflects also at the top and bottom of the band-edge, generating a square signal. We observed strong acoustic resonances at frequencies of 18 kHz, 37 kHz and 61 kHz. The peak-to-peak amplitude was measured for these frequencies as a function of the voltage applied to the piezoelectric, see Fig. 13(b). The most efficient frequency was 61 kHz, and the responses at 18 kHz and 37 kHz were quite similar. Taking into account the results shown in Fig. 13(b) and the width of the band-edge, 42 pm, the modulation efficiency (i.e. wavelength shift per unit volt) was estimated, giving 7 pm/V at 18 kHz and 37 kHz, and 16 pm/V at 61 kHz.

The switching speed is one of the key parameters of any modulator intended to be utilized as Q-switching element in a fiber laser, being desirable to be as high as possible. In this modulator, the switching time depends on the AC voltage amplitude, and it becomes shorter as the voltage is increased, as shown in Fig. 13(a). Switching times of the order of a

few microseconds were achievable. Finally, although the acoustic generator was designed for the excitation of longitudinal waves, we also observed flexural waves in the resonator when large voltages were applied to the piezoelectric. A large number of flexural standing waves, spaced fractions of kHz, were observed in the range from 0 to 100 kHz. These resonances gave rise to light modulated at double frequency of the electrical excitation and exhibited relatively low amplitude. The aforementioned modulator uses an acoustic resonator, which enhances the interaction between acoustic waves and the FBG. The fundamental mechanical resonance at 18 kHz had a *Q* factor of 1300. With respect to an un-clamped configuration based on traveling acoustic waves, the use of an acoustic cavity increases the modulation efficiency, but it restricts the operation of the modulator at the resonant frequencies of the cavity. A modulator based on traveling acoustic waves would allow, in principle, tuning continuously the modulation frequency, but a large voltage would be required and important thermal effects would damage the acoustic transducer.
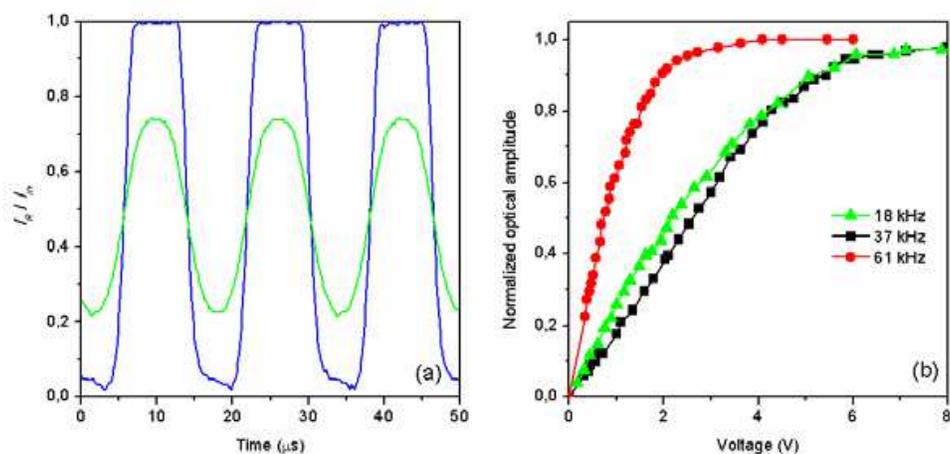
Fig. 13. (a) Light reflected from the band-edge of the grating when an AC electric signal of 61 kHz and peak-to peak amplitude of 4.6 V (green) and 14 V (blue) were applied to the piezoelectric. (b) Light modulation amplitude as a function of voltage for three different resonant frequencies
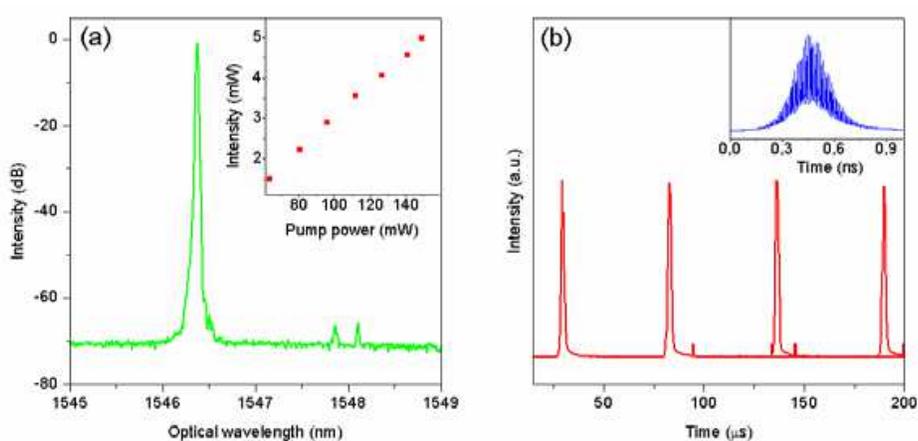
Fig. 14. (a) CW emission spectrum at 135 mW pump power; the inset shows the output CW power versus pump power. (b) Pulse train at 18 kHz repetition rate; the inset shows a single light pulse measured with a 1 GHz bandwidth photodetector, pump power of 80 mW
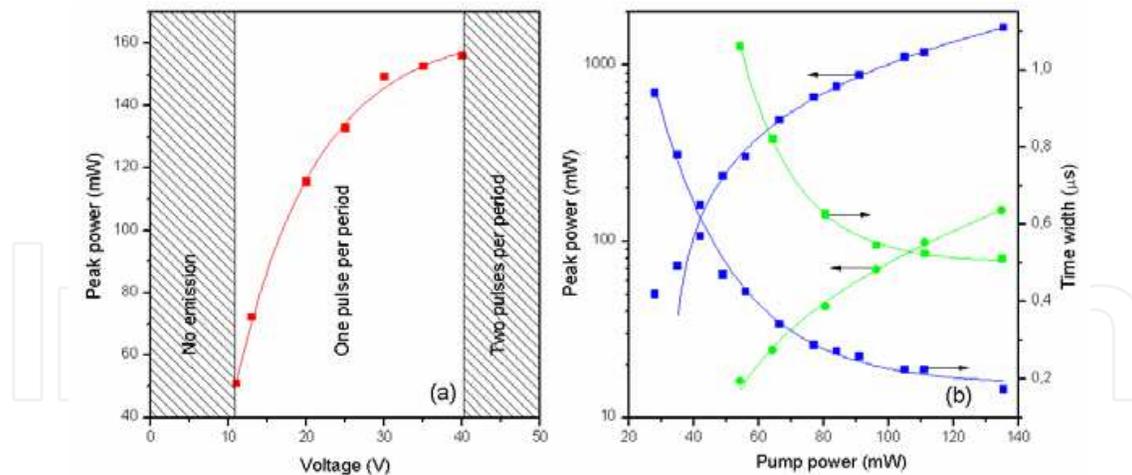
Fig. 15. (a) Pulse peak power as a function of the applied voltage to the piezoelectric (75 mW pump power, 18 kHz repetition rate). (b) Pulse peak power and pulse width as a function of pump power, for repetition rates of 18 kHz (blue) and 37 kHz (green). Voltage applied to the piezoelectric 24 V

The gain of the *Q*-switched all-fiber laser was provided by 0.3 m of an erbium-doped fiber containing 1000 p.p.m. Er^{3+}, with a cut-off wavelength of 965 nm, and a numerical aperture of 0.23. The active fiber was pumped through a WDM coupler by a pigtailed laser diode emitting at 979 nm, providing a maximum pump power of 140 mW. The Fabry–Perot cavity length was of 1.2 m. A translation stage was used for tuning the reflection band of FBG_2 closer to the short-wavelength band-edge of FBG_1, allowing full overlapping between both bands with moderate voltages being applied to the piezoelectric. In this arrangement, the longitudinal standing elastic wave causes periodic optimization of the *Q* factor of the laser cavity and, as a result, strong pulses are emitted at the repetition frequency of the acousto-optic modulation, when the fiber is pumped. The CW features of the fiber laser are shown in Fig. 14(a). The laser line was narrower than 20 pm (resolution limit of our measurement system), a signal-to-noise level as high as 70 dB was obtained. The efficiency and the threshold were 3 % and 25 mW, respectively. Figure 14(b) shows a pulse train emitted by the laser at a repetition rate of 18 kHz. At high pump powers each *Q*-switched pulse breaks into a train of narrower, 8 ns wide, sharp pulses (see inset). The frequency of this modulation, 83 MHz, coincides with the frequency mode-spacing of the laser cavity, which indicates beating between longitudinal cavity modes. We observed that the modulation amplitude of this high frequency component was affected by variations in pump level and repetition rate. This apparent passive mode-locking response has been previously reported repeatedly in both, passively and actively *Q*-switched fiber lasers (Philippov et al., 2004; Andersen et al., 2006). Figure 15(a) shows the peak power of the *Q*-switched pulse as a function of the applied voltage to the piezoelectric. Three regions can be clearly distinguished. For low voltages applied to the piezoelectric there is not emission, since the wavelength shift of FBG_1 is not enough to overlap the reflection band to FBG_2. As the applied voltage increases, there is a *Q*-switched pulse per period. For voltages close to the lower limit, the overlapping between both gratings is only partial and the laser is only a small amount above threshold, so weak pulses are emitted. As the voltage is increased, the gratings overlap further and the peak power increases. A steady state is reached when the voltage amplitude is high enough to obtain complete overlapping between the two reflection bands. If the applied voltage is increased further, the cavity stays in the high *Q* state longer

and more than one Q-switched pulse is emitted per period. When changing the pump power and/or repetition rate, the upper and lower AC voltage limits vary, but the trend is preserved. Finally, the effect of pump power on the Q-switched pulses, for repetition rates of 18 and 37 kHz, is shown in Fig. 15(b). The pump power threshold at each frequency was 27 mW and 53 mW, respectively. Above threshold, the peak power increases with pump power, and there is a corresponding reduction of the pulse width. No evidences of peak power saturation were observed within the pump power range of our experiments. Pulses of 1.6 W peak power and 172 ns width were obtained at 18 kHz repetition rate and 135 mW pump power.

3.2 Mode-locking and Q-switching mode-locking by acousto-optic interaction in a fiber Bragg grating in the short-wavelength regime

In this subsection we discuss another mechanism developed by our group to mode-lock an all-fiber laser (Cuadrado-Laborde et al., 2009a, 2010a). This is based on the acousto-optic super-lattice modulation, and it is an example of the interaction of longitudinal acoustic waves and Bragg gratings in the short-wavelength regime (Liu et al., 1997, 1998). In the following, we start by reviewing the behavior of the acousto-optic super-lattice modulator, subsection 3.2.1. Then, we show the use of this device as mode-locker, by showing two different mode-locked lasers, either by driving the acousto-optic modulator by standing or travelling acoustic waves, subsections 3.2.2 and 3.2.3, respectively. The possibility to reach simultaneous Q-switching and mode-locking is also discussed in these subsections.

3.2.1 The fiber Bragg grating based acousto-optic modulator

The spectral response of the original FBG in this acoustical regime shows new –and narrow– reflection bands symmetrically at both sides of the original Bragg wavelength (Liu et al., 1997, 1998). The position of these sidebands can be controlled by varying the frequency at a slope of 0.15 nm /MHz and 0.30 nm /MHz for the first and second order sideband, respectively. The strength of the reflection bands, on the other hand, can be controlled independently by varying the voltage applied to the piezoelectric. Since these sidebands can be regarded as weak ghosts of the strong permanent Bragg grating, its FWHM bandwidth is that of a weak Bragg grating of the same length (Liu et al., 1997). Figure 16 shows the setup for a typical reflectivity measurement on an AOSLM. The AOSLM in turn is composed of an RF source, an electrical RF amplifier, a piezoelectric disk, a silica horn, and a FBG. The tip of the silica horn was reduced by chemical etching to the same diameter of FBG –125 μm– and subsequently fusion-spliced to the fiber. The uniform and non-apodized grating was written in photosensitive fiber using a doubled argon laser and a uniform period mask; the FBG was 120 mm long. The reflection properties of the AOSLM were investigated by illuminating the FBG through an optical circulator with a broadband light source, and detecting the reflected light with an optical spectrum analyzer (OSA). Figure 17(a) shows the reflectivity of the unperturbed FBG –i.e. without electrical signal applied to the piezoelectric– and with an electrical signal applied to the piezoelectric of 4.55 MHz and 16 V (whenever we refer to voltages throughout this chapter, it is a peak-to-peak measurement). The presence of the sidebands symmetrically positioned around the Bragg wavelength is clearly discernible. Further, these sidebands are produced either by standing or travelling acoustic waves. However, the light reflected by the sidebands in each case behaves differently. When travelling acoustic waves are used –by dumping the end of the FBG opposite to the silica horn for example with a drop of oil–, the light reflected on these sidebands is completely downshifted or upshifted by the frequency of the acoustical signal, depending if the

reflection was in the long or short-wavelength sideband, respectively (Liu et al., 1997, 1998). Together with this and as a function of the instantaneous phase of the acoustic signal, there is also present an amplitude modulation at the frequency of the acoustical signal. Figure 17(b) shows the measurement performed by tuning a laser diode to the center of the short-wavelength sideband and measuring the reflected light. As expected, the amplitude modulation is at the same frequency of the electrical signal used to drive the piezoelectric. On the other hand, when standing acoustic waves are used –by clamping the end of the FBG opposite to the silica horn– the sidebands raise and fall at twice the frequency of the electrical signal (Cuadrado-Laborde et al., 2009a). Further, in principle, for a perfect acoustical reflection, the light reflected by the sidebands does not experiment any Doppler shift, as opposed to the previous case when travelling acoustic waves are used. Figure 17(c) shows the measurement performed by tuning a laser diode to the center of the short-wavelength sideband and measuring the reflected light. Now the optical modulation frequency is two times the acoustical signal frequency. To summarize, an AOSLM can be driven in two different regimes, either by using travelling or standing acoustic waves. In both cases we can use it as an amplitude modulator. However in the first case –travelling acoustic waves– the light reflected on the sidebands is modulated at the same frequency of the acoustical signal, whereas in the second case –standing acoustic waves– it is modulated at two times this frequency, respectively.
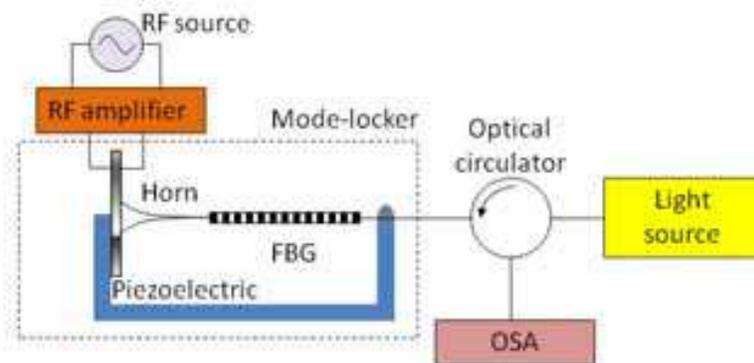

Fig. 16. Setup for the characterization of the acousto-optic super-lattice modulator; OSA stands for optical spectrum analyzer, FBG for fiber Bragg grating and RF for radio-frequency
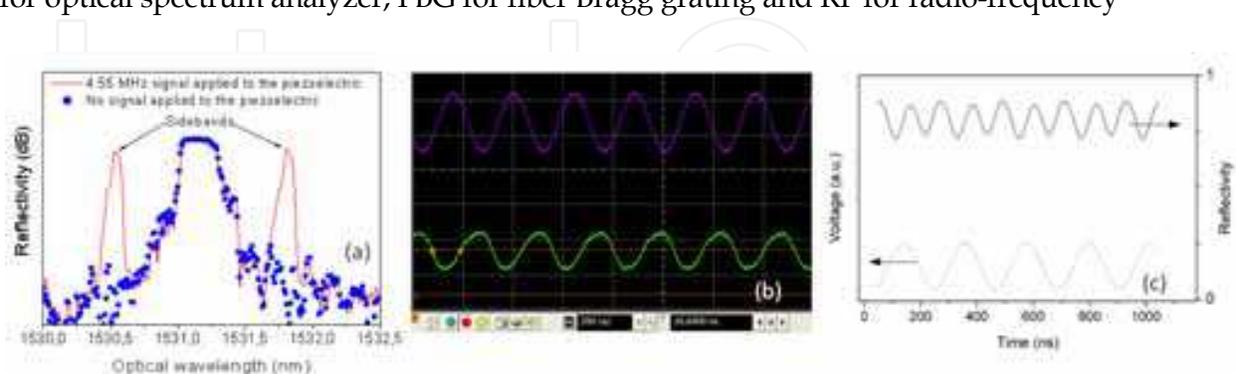

Fig. 17. (a) Reflectivity of the fiber Bragg grating with and without electrical signal applied to the piezoelectric (4.55 MHz and 16 V peak-to-peak). (b) Optical signal reflected by the short-wavelength sideband when travelling acoustic waves are used (lower trace) and RF voltage applied to the piezoelectric (4.11 MHz and 16 V, upper trace). (c) Same as in (b), but for standing acoustic waves (4.55 MHz and 16 V, dotted curve)
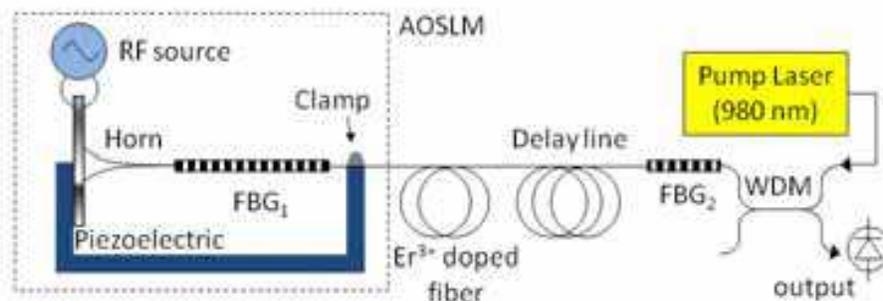
Fig. 18. Setup of the mode-locked all-fiber laser by using an acousto-optic supper-lattice modulator (AOSLM) as mode-locker

3.2.2 All-fiber actively mode-locked laser with a fiber Bragg grating based acousto-optic modulator driven by standing acoustic waves

Now, we show the use of the amplitude modulation induced by standing acoustic waves in the AOSLM to mode-lock an all-fiber laser (Cuadrado-Laborde et al., 2009a, 2010a). The setup proposed for the standard mode-locking laser is schematically illustrated in Fig. 18. The gain was provided by an erbium-doped fiber (EDF) containing 300 parts per million (ppm) of Er^{3+}, with a cut-off wavelength of 939 nm, and a numerical aperture of 0.24. The active fiber was pumped through a WDM coupler by a pigtailed laser diode emitting at 976 nm, providing a maximum pump power of 160 mW. The acousto-optic super-lattice modulator and a short delay line followed by a second fiber Bragg grating FBG_2 were fusion-spliced at each end of the active fiber. FBG_2 (10 mm long and with a Bragg wavelength of 1530.2 nm) was written with a uniform period in a photosensitive fiber using a doubled argon laser and a uniform period mask. The Fabry-Perot cavity was established once the reflection band of FBG_2 is made to match the short wavelength sideband of the FBG_1 of the AOSLM, i.e. 1530.5 nm, by straining it with a translational stage (see Fig. 18). The delay line length must be selected to match the round-trip time with the reciprocal of the optical modulation frequency, which in turn is twice the electrical frequency applied to the piezoelectric. Since the selected piezoelectric operation point for the piezoelectric was 4.55 MHz, this results in a cavity length of 11.4 m. However, fine tuning of the electrical frequency was required to achieve mode-locking.

Figure 19(a) exemplifies the laser behavior showing the train of optical pulses generated, at a frequency rate of 9 MHz (50 GHz bandwidth oscilloscope). Figure 19(b) shows a single optical pulse; the timing jitter was measured to be 40 ps (RMS). The pulses of this laser are best fitted by a $sech^2$ function, which is in accordance with earlier amplitude modulated mode-locking theory. Further, the dispersion measurements of the different fibers we used to form the laser cavity show that both kind of dispersion coexist, from the anomalous dispersion of the delay line to the normal dispersion of the EDF. For this type of dispersion-mixed cavities, the analytical steady-state solution is expected to be also of the $sech^2$ type (Belanger, 2005), which adds further evidence in the same direction. The emission linewidth was measured using a high resolution optical spectrum analyzer (BOSA-C, Aragón Photonics, resolution of 80 fm). Figure 19(c) shows the spectrum of the optical pulses shown in Fig. 19(b). The high resolution of the optical spectrum analyzer permits a direct observation of the individual cavity modes separated by 9 MHz, see the inset of Fig. 19(c). The measured 3-dB linewidth results in 2.8 pm, i.e. 360 MHz at 1530.5 nm. On the other side, the optical pulses have a temporal width of 780 ps, so according to the Fourier-transform-

limited relation for a sech² pulse, time-bandwidth product of 0.315 (Wada et al., 2008), its bandwidth cannot be lower than 380 MHz. From the comparison between this last value and the linewidth measurement, we conclude that the optical pulses of our modelocked laser are transform-limited, i.e. un-chirped. A brief digression is in order here, the Fourier-transform-limited relation for Gaussian pulses with a time-bandwidth product of 0.44 (Kuizenga & Siegman, 1970; Wada et al., 2008), would result in a much higher linewidth (564 MHz), which is in contradiction with our spectral measurements. As a consequence, the fitting of the temporal pulses, see Fig. 19(b), the application of the Fourier-transform-limited relations, and dispersion measurements together with previous theoretical work, seems to corroborate a sech² nature for the emitted pulses.
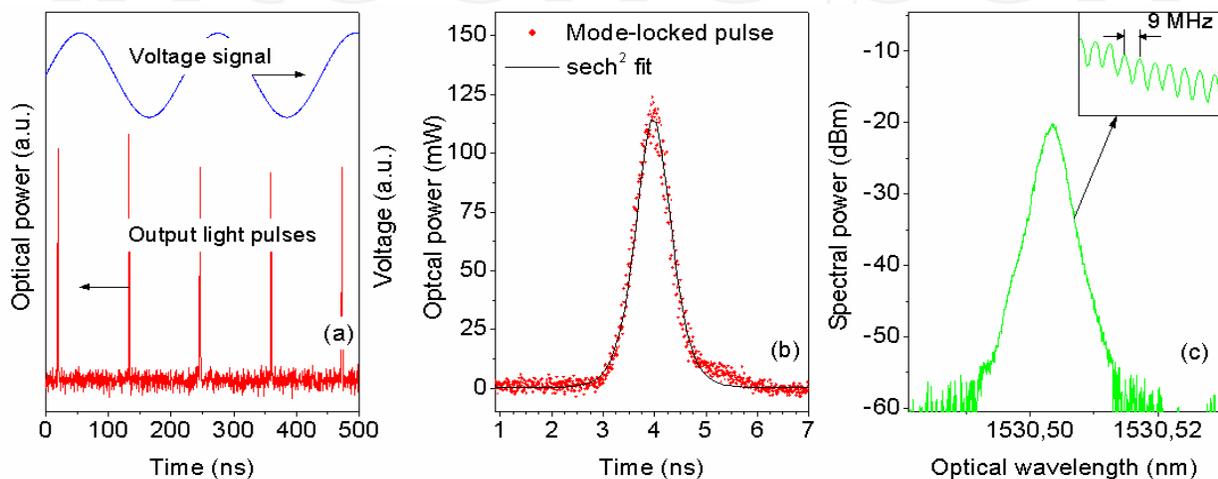
Fig. 19. (a) Voltage signal applied to the piezoelectric at 4.55 MHz and 16 V, and its corresponding modelocked train of pulses generated at twice this frequency with a pump power of 160 mW. (b) A single optical pulse and its corresponding fitting by a sech² function. (c) Optical spectrum of the output light pulses shown in (b); the inset shows the cavity modes distant by 9 MHz
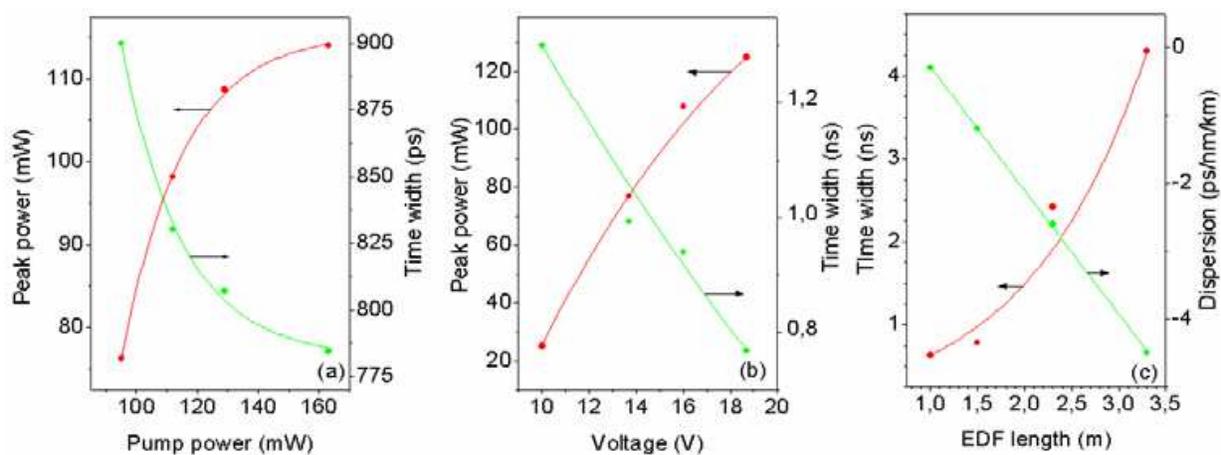

Fig. 20. (a) Peak power and pulse width of the optical pulses as a function of the pump power. (b) Peak power and pulse width of the output light pulses as a function of the voltage applied to the piezoelectric, for a pump power of 160 mW. (c) Pulse width of the output light pulses, as a function of the EDF length, for a fixed pump power of 160mW, additionally, the average dispersion of the cavity is also shown for each EDF length

Now we will show the variation in the pulse`s parameter as typical variables are changed. First we analyze the optical pulse's peak power and temporal width as a function of the pump power, which is shown in Fig. 20(a). A smooth variation of the pulse width with pump power can be observed, before reaching the gain saturation. A higher available pump power would allow additional axial modes to contribute, increasing the spectral bandwidth, and thereby decreasing the pulse´s width. Next, we analyzed the variation in the pulse`s parameters as a function of the modulation voltage. The intensity of the reflection sidebands of the AOSLM can be dynamically controlled by varying the voltage applied to the piezoelectric as we explained before in subsection 3.2.1. This voltage controls the amplitude of the propagating acoustic wave and the amplitude of the standing wave, as a function of the reflection at the clamp. Thus, as opposed to mode-locking by bulk acousto-optic or electro-optic modulators, here the reflectivity and the modulation depth are intrinsically linked, i.e. when the applied voltage increases, both the reflectivity and the modulation amplitude increase. Figure 20(b) shows the peak power and time width, respectively, as a function of the voltage applied to the piezoelectric. At lower reflectivities and modulation amplitudes, the peak power diminishes, whereas the time width increases. According to Eq. (1), the pulse width and the modulation depth are inverse parameters, and in turn the later rises with the applied voltage. However, the pulses shorten very slowly with the increased modulation strength; hence this shortening procedure is generally discouraged (Kuizenga & Siegman, 1970). One can conclude that further increase of the voltage might improve the pulse parameters, but it is not likely to lead to a great enhancement in terms either of peak power or temporal width. We analyzed also the influence that dispersion has on the pulse`s parameters, when the average dispersion of the cavity is changed. The dispersion for each type of optical fiber used in the setup was measured by the frequency-domain modulated-carrier method. The resulting average dispersion of this cavity is normal and its value is −1.2 ps/nm/km. Next, the optical fiber of the delay line –the Corning LEAF fiber– was replaced by a normal dispersion fiber –Fibercore SM980– leading to a lower (normal) overall dispersion of −5.8 ps/nm/km. With the new delay line, a higher pump reaches the EDF, since a better effective area compatibility is insured throughout the different fibers of the system –in fact, unlike LEAF fiber, the SM980 insures single-mode propagation of the pump power–. As a result, output pulses have higher peak power and shorter time width than in the previous configuration. In this way, optical pulses with temporal width and peak power of 640 ps and 160 mW, respectively, were obtained. These pulse parameters represent an improvement of 18% and 28% with respect to the previous configuration. Finally, in order to reverse the sign of the average dispersion of the cavity, we used an SMF28 optical fiber for the delay line, resulting in an average –anomalous– dispersion of 9.8 ps/nm/km. In this case, we did not observe mode-locking lasing. One reason for this could be motivated by the large average dispersion introduced within the cavity, since modelocked fiber lasers usually works with close-to-zero average dispersion cavities. Finally, the change on the pulse parameters was measured as a function of the EDF length –ranging from 0.5 to 3.3 m–, but keeping a constant cavity length of 11.4 m, by adjusting each time the length of LEAF fiber. The average dispersion remains normal regardless of the amount of EDF used, ranging from −0.3 ps/nm/km up to −4.5 ps/nm/km. The temporal pulse width as a function of the EDF length is shown in Fig. 20(c), for a fixed pump power of 160 mW. This figure includes the average dispersion of the cavity as a function of the EDF length. A direct relationship can be observed between the EDF length, the dispersion, and the time width of the pulses, with a minimum of 630 ps obtained for an EDF length of 1 m. This kind of interplay between gain and time width

agrees with Eq. (1). Further narrowing of the optical pulses could not be reached by this trend, since no mode-locking lasing was observed with 0.5 m of EDF and the available pump power, as a result of insufficient cavity gain. Finally, we also developed the ytterbium-doped fiber version of this laser, with equally satisfactory results (Villegas et al., 2011).
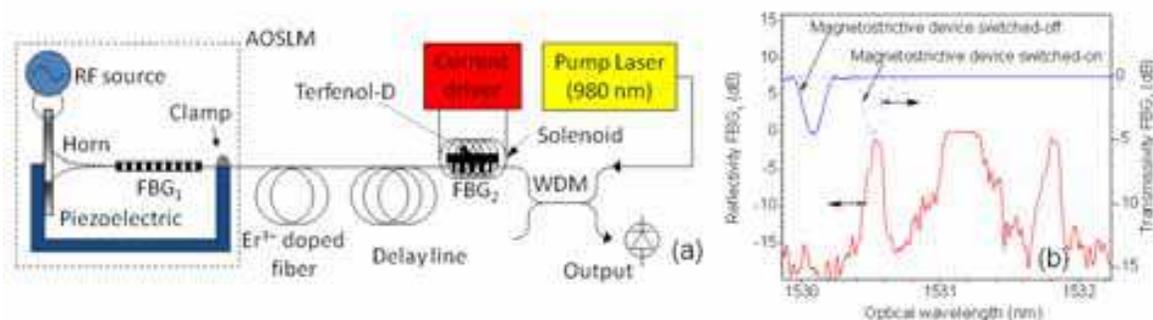

Fig. 21. (a) Q-switched mode-locked all-fiber laser setup when the AOSLM is driven by standing acoustic waves. (b) Reflection spectrum of the AOSLM when an RF signal of 4.55 MHz and 16 V is applied to the piezoelectric (left ordinate). Transmittance of FBG_2 (solid curve) when the magnetostrictive device is switched-off; the dotted curve shows the new spectral position of FBG_2 when the magnetostrictive device is switched-on (right ordinate)

Until now we have discussed the standard mode-locking operation. Now we demonstrate the possibility to simultaneously Q-switch and mode-lock, actively and independently. By combining both operations in a single laser, a superior performance is achieved with higher peak powers compared with ordinary mode-locked lasers, but almost the same pulse width as in a mode-locked laser is retained. Thus, the peak power of the central pulses of the mode-locked train, underneath the Q-switched envelope, can be greatly enhanced. The increased peak power provided by the Q-switching technique can be advantageous in applications such as wavelength conversion or super-continuum generation. It is worth to say, that any passive mechanism is used in this setup, neither for Q-switching nor for mode-locking. To this end, we design a solution for actively Q-switching, while simultaneously mode-locking, preserving the all-fiber configuration. This solution is based on fiber Bragg grating fast modulation using a magnetostrictive device. This feature provides a direct control of the repetition rate and a fully-modulated train of modelocked pulses. To the best of our knowledge, this was the first doubly active Q-switching mode-locking strictly all-fiber laser presented (Cuadrado-Laborde et al., 2009b). The setup of our doubly-active Q-switching mode-locking all-fiber laser is shown in Fig. 21(a). It is basically the same as it was described before for the standard mode-locking and shown in Fig. 18, with the same length of EDF and delay line, except by the magnetostrictive device controlling the FBG_2, see Fig. 21(a). It is composed of a 15 mm long (1 mm² cross-section) magnetostrictive rod of Terfenol-D bonded to the FBG_2. The rod and the fiber were placed inside a small coil driven by an electronic circuit designed to drive square current pulses with amplitudes up to 260 mA of any required duty cycle. Figure 21(b) shows the spectral positions of both FBGs –i.e. the FBG of the AOSLM and FBG_2, which helps understand the operation principle of this laser also. When the magnetic pulses generated in the solenoid stretch FBG_2, its central wavelength is brought to match the short-wavelength sideband of FBG_1 for a short period of time, which results in an increased Q-value. In this way by modulating the coil current with a given Q-switched frequency, the Q-factor is actively modulated at the same frequency. The

magnetostriction has a low pass frequency response and, consequently, presents the advantage to permit a continuous tuning of both the *Q*-switched repetition rate and the duty cycle of the modulation pulses. The dependence of the wavelength shift with the coil current was measured by illuminating FBG_2 with a tunable laser source and detecting the reflected light. A quasi-linear behavior was observed, as a result of using moderate magnetic fields.
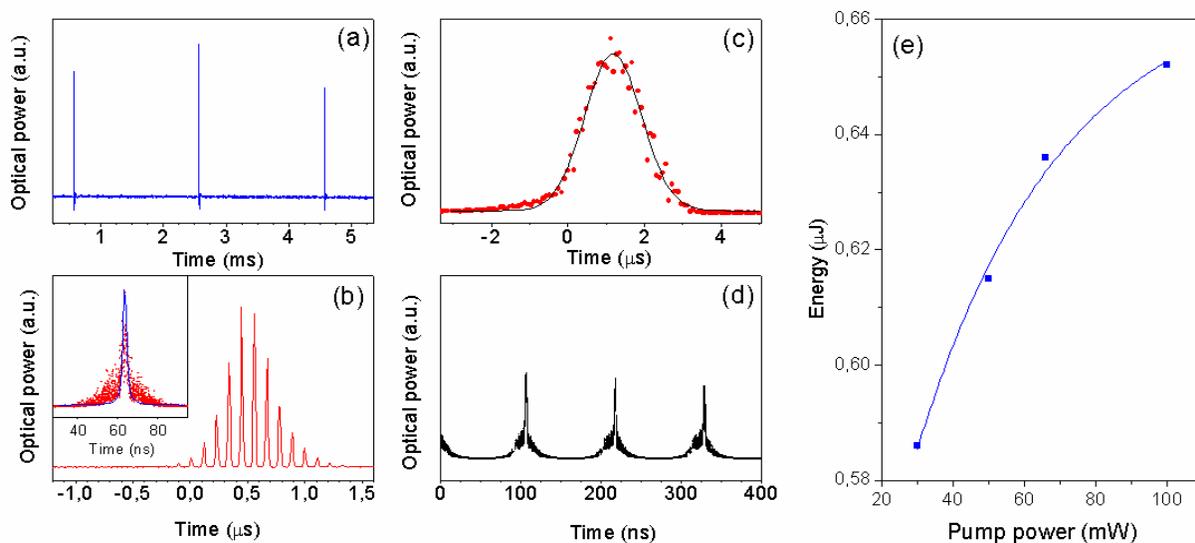

Fig. 22. (a) *Q*-switched mode-locked train of pulses at a *Q*-switching frequency of 500 Hz. (b) Single *Q*-switched pulse enveloping a train of 12–14 modelocked pulses; the inset shows a single modelocked pulse. (c) Single *Q*-switched pulse with no mode-locked. (d) Mode-locking operation of the laser without *Q*-switching. In all cases, the pump power was 70mW. (e) Energy of the *Q*-switched mode-locked pulses as a function of the pump power for a *Q*-switching repetition rate of 500 Hz

Now we discuss the *Q*-switching mode-locking laser operation. The laser emission wavelength was in 1530.55 nm, since the overlapping between the short-wavelength sideband of FBG_1 and the shifted position of FBG_2 takes place at this wavelength, see Fig. 21(b). Figure 22(a) exemplifies the *Q*-switched mode-locked laser behavior showing the train of optical pulses generated for a pump power of 70 mW. The optical *Q*-switched mode-locked pulses are 2 ms apart, since the repetition rate of the train of voltage pulses applied to the current driver was of 500 Hz. Figure 22(b) shows a single *Q*-switched envelope with a FWHM of 550 ns; it has between 12 and 14 fully-modulated modelocked pulses, with the expected temporal separation of 110 ns. However, the individual short pulses are broadened due to the limited bandwidth and sampling rate of the oscilloscope. In order to measure the FWHM of the individual short pulses, a 50 GHz sampling oscilloscope was used. In this case, the large difference between the *Q*-switching and mode-locking frequencies make difficult to trigger properly the oscilloscope. Even so, relatively good traces were recorded as the one depicted in the inset of Fig. 22(b). As we discussed before when we presented the standard mode-locking regime, the tuning sensitivity between the RF signal applied to the piezoelectric and the cavity round trip is not too critical in this setup. Only when the detuning is considerably –e.g. by a few kHz–, the pulse clearly deteriorates. Figure 22(c) shows the *Q*-switched pulse obtained by avoiding the mode-locking pulse formation, just by detuning the applied voltage to the piezoelectric by 10 kHz, in this way only the *Q*-switching operation is allowed within the cavity. As expected, the *Q*-switched pulse

reproduces the waveform of the envelope of the *Q*-switched mode-locked pulses shown in Fig. 22(b), but with a much lower peak power (by a factor of ~4×10^{-3}) and an increased temporal width. The transition from the fully-modulated *Q*-switched mode-locked pulses to the pure *Q*-switching operation –i.e. from Fig. 22(b) to 22(c)– is progressive as we detuned the voltage applied to the piezoelectric. Finally, Fig. 22(d) shows the behavior of this laser when turning off the active *Q*-switching, i.e. standard mode-locking operation of the laser. To this end, a DC current was driven to the coil of the magnetostrictive device, in order to achieve a stationary overlap with the short wavelength sideband of the AOSLM. The trace of Fig. 22(d) was recorded with the 1 GHz oscilloscope. In this case, the thermal effects produced by the DC current made difficult an optimum and stable adjustment of FBG$_2$. The comparison of Figs. 22(b) and 22(d), illustrates the improved performance of the laser in terms of peak power when both *Q*-switching and mode-locking are operating. The energy of a *Q*-switched train of pulses, as that reported in Fig. 22(b), as a function of the pump power is shown in Fig. 22(e). This energy was measured directly with a pyroelectric detector. At high pump powers, the energy of the *Q*-switched mode-locked train of pulses reach gain saturation. Thus, a peak power higher than 250 W can be calculated for the central pulses of a train with energy of 0.65 μJ, assuming that the mode-locked pulses are 1 ns width. This result demonstrate a dramatic enhancement in comparison with the peak power achieved when the laser was operated in standard mode-locking regime (Cuadrado-Laborde et al., 2009a), since the ratio is higher than 2×10^3.
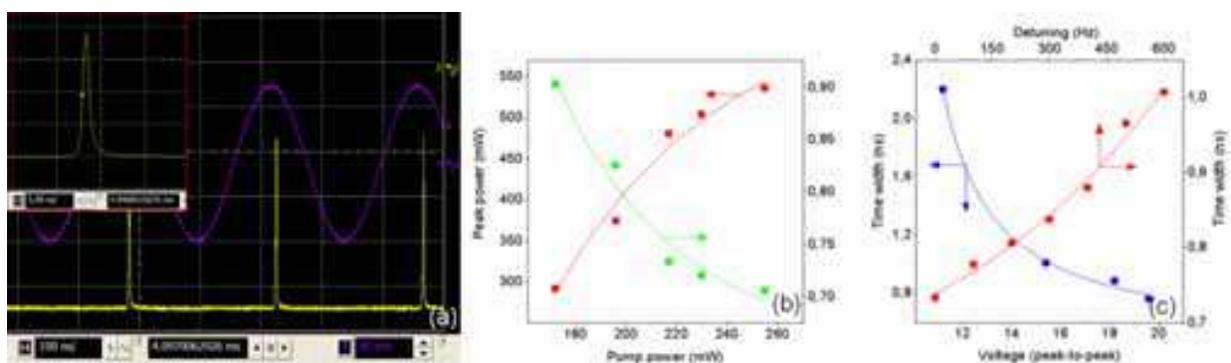

Fig. 23. (a) Oscilloscope traces of the sinusoidal electrical signal applied to the piezoelectric at 4.1 MHz repetition rate and 16 V (upper trace), and the train of optical pulses generated (lower trace); a pump power of 230 mW was used. The inset shows the detail of a single pulse of the optical train, with a FWHM of 720 ps and a peak power of 500 mW. (b) Peak power and pulse width (FWHM) of the optical pulses as a function of the pump power (solid and dotted curves, respectively). (c) Pulse width of the optical pulses when the applied voltage to the piezoelectric is varied, and when the frequency of the electrical signal is varied

3.2.3 All-fiber actively mode-locked laser with a fiber Bragg grating based acousto-optic modulator driven by travelling acoustic waves

The setup of the mode-locking laser driven by travelling acoustic waves is essentially the same described in Fig. 18, but with two important differences. First, the pigtailed laser diode emitting at 976 nm provides now a –higher– maximum pump power of 410 mW. Second, the modulation frequency is now at the same frequency of the acoustical signal (Cuadrado-Laborde et al., 2010b), since now we use travelling acoustic waves, see Subsection 3.2.1. Then, the delay line length is now much larger, because we must match the round-trip time

with this frequency, which is lower. Since the selected piezoelectric operation point was of 4.1 MHz; then it results in a cavity length of 25 m –compare this with the 11.4 m of cavity length used before. Apart from the 1.4 m of EDF, the cavity was constructed entirely with Fibercore SM980 fiber, this result in an average dispersion of –4.9 ps/nm/km (i.e. normal). Figure 23(a) exemplifies the laser behavior showing the sinusoidal electrical signal applied to the piezoelectric at a frequency rate of 4.1 MHz and the train of optical pulses generated at the same frequency. The inset shows a detail of a single optical pulse with a temporal width (FWHM) of 710 ps. Once mode-locking was reached, the polarization controllers were adjusted in order to obtain the minimum pulse width.

The emission linewidth was measured using a classical heterodyne configuration (Galtarossa et al., 1993). To this end, a tunable laser was used as local oscillator, with a 100 kHz linewidth. The output of this laser was superimposed to the optical pulses of the modelocked laser, through a 1550 nm 50/50 coupler. The beat signal at the coupler output was detected with a 45 GHz bandwidth photodetector, and analyzed with a 2.5 GHz oscilloscope. This results in a linewidth for the mode-locked laser of 560 MHz for a 900 ps (FWHM) pulse, measured directly in the spectrum at –3 dB. Again, we found that the output pulses of this laser are best fitted by a $sech^2$ function rather than with a Gaussian function. From the Fourier-transform-limited relation for a $sech^2$ pulse, its time-bandwidth product cannot be lower than 0.315 (FWHM) (Wada et al., 2008). Since we obtain 560 MHz × 900 ps = 0.504, we conclude that the optical pulses of our modelocked laser could have some moderate degree of chirp.

According to Eq. (1), the pulse duration is limited by a variety of factors in an active modelocked laser. From these parameters, we believe the narrow spectral bandwidth of the AOSLM $\Delta\lambda$ plays a key role in this setup. As we explained before, these sidebands can be regarded as weak ghosts of the strong permanent Bragg grating, its FWHM bandwidth is that of a weak Bragg grating of the same length (Liu et al., 1997), namely $\Delta\lambda = 1.39\lambda^2 / (\pi L n_0)$, where L is the fiber length and n_0 is the modal effective index. For the grating used in this chapter, with L = 120 mm, at λ = 1530 nm, this translates into $\Delta\lambda$ = 6 pm, which is equivalent to 770 MHz at the operation wavelength of this laser (1530.5 nm). As a rough estimation, since the cavity modes are distant 4.1 MHz, it is easily seen that this AOSLM only is able to lock a few percent of the axial modes available by the medium gain, namely 770 MHz /4.1 MHz = 192 modes (FWHM). If we assume for the output pulses of this laser a $sech^2$ envelope, then this parameter alone determines a lower limit for the pulse width around 0.315 /770 MHz = 410 ps. Therefore, we believe that narrower pulses can be reached by broadening the sidebands of the AOSLM in order to lock additional axial modes. The optical pulse's peak power and temporal width as a function of the pump power are shown in Fig. 23(b). A smooth variation of the pulse width with pump power can be observed, before reaching the gain saturation. Fig 23(c) shows the time width as a function of the frequency detuning. The behavior was asymmetric, i.e. it depends if the detuning was positive or negative. Once mode-locking is reached and the PC adjusted to get the minimum pulse width, a small detuning in either direction does not modify the pulse width –e.g. up to a few tens of Hertz, as expected for amplitude modulation mode-locking (Kuizenga & Siegman, 1970). However, when the detuning is considerably higher, a positive detuning continuously broadens the time width, whereas for a negative detuning, the mode-locking is rapidly lost, and the pulses drop out. We believe this asymmetry could be caused by the non-flat frequency response of the piezoelectric. We conclude this subsection by analyzing the behavior of this laser when the voltage applied to the piezoelectric changes. Figure 23(c)

shows the influence on the time width of the optical pulses with the voltage applied to the piezoelectric. For higher voltages, the time width decreases; further narrowing by this trend appears to finish when the reflectivity of the sideband approaches the maximum (in addition, 20 V was the maximum voltage provided by the electrical amplifier used to drive the piezoelectric). Within the range of voltage available in our experiments, both the reflectivity and the modulation amplitude increase continuously. This is consistent with Eq. (1), by which the time width is inversely related with both, the modulation depth and the reflectivity.
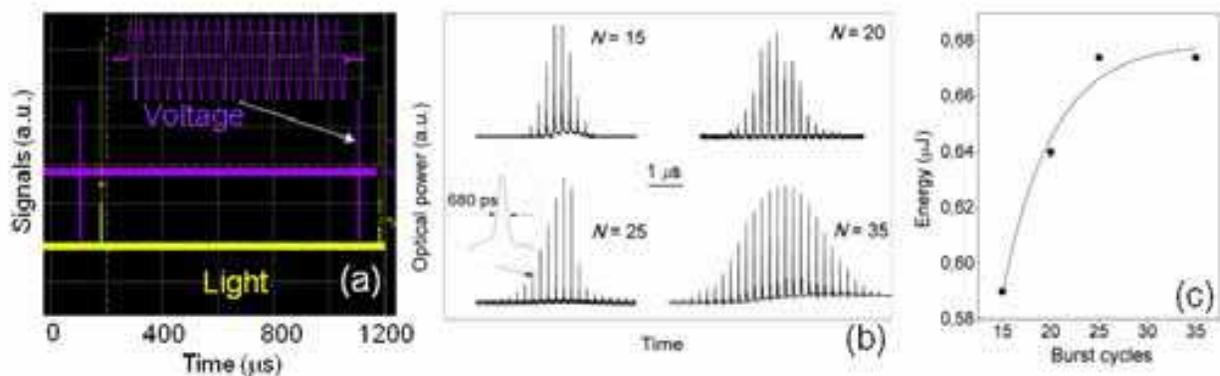
Fig. 24. (a) Voltage signal applied to the piezoelectric and *Q*-switched mode-locked train of pulses generated for a 1 kHz *Q*-switching repetition rate; the inset shows a detail of the burst signal. (b) Single *Q*-switched mode-locked pulses enveloping a train of modelocked pulses for different burst cycles; the inset shows a single-shot capture of a single modelocked pulse with a FWHM of 680 ps. (c) Energy of the *Q*-switched mode-locked pulses as a function of the cycles contained in the burst for a fixed *Q*-switching frequency of 500 Hz and a pump power of 270 mW

The most significant advantage of using travelling instead of standing acoustic waves is determined by the possibility to actively *Q*-switch this modelocked laser simply by launching to the grating a burst acoustical wave (Cuadrado-Laborde et al. 2010b). Therefore, the setup is exactly the same as the reported above for the standard mode-locking regime driven by travelling acoustic waves. The burst signal consists of an integer number of sinusoidal acoustical cycles *N*. Figure 24(a) shows the burst voltage signal applied to the piezoelectric together with the *Q*-switched mode-locked train of pulses generated, at a frequency rate of 1 kHz. Figure 24(b) shows several *Q*-switched mode-locked pulses as a function of *N*. When *N* is low, *Q*-switched mode-locked is not reached. For higher *N*, *Q*-switched mode-locked is reached and the emission is allowed. For example, the left bottom corner of Fig. 24(b) shows a single *Q*-switching envelope with a FWHM of 1.4 µs for *N* = 25; it has between 16 and 18 fully-modulated modelocked pulses, with the expected temporal separation given by 1/4.1 MHz = 244 ns. The inset shows a single-shot capture of a modelocked pulse within this train with a temporal width of 680 ps. As observed, the *Q*-switched mode-locked pulses of this laser have excellent inter-pulse characteristics. The energy of a *Q*-switched mode-locked train of pulses, as a function of *N* is shown in Fig. 24(c). This energy was measured directly with a pyroelectric detector. As expected, for a longer burst signal, the energy of the *Q*-switched mode-locked train of pulses increases, until it reaches saturation. Thus, a peak power higher than 200 W can be calculated for the central pulses of a train with energy of 0.68 µJ, assuming that the modelocked pulses are 680 ps width. This result clearly demonstrates the degree of enhancement in comparison with

the peak power achieved when the laser was operated in the standard mode-locking regime, since the ratio is higher than 4×10^2.

3.3 Photonic true-time delay-line by acousto-optic interaction in a fiber Bragg grating in the short-wavelength regime

A photonic true-time-delay (PTTD) line is an optical device that permits to vary the group delay of an optical signal. The ideal PTTD line should exhibit fast tuning within a broad range of time delay values. PTTD lines attract much attention due to an increasing number of applications such as the control of phased array antennas (Liu et al., 2002; Perez-Millán et al., 2004; Italia et al., 2005;), tunable microwave band-pass filters (Capmany et al., 2005), buffering and packet synchronization (Li et al., 2007; Caucheteur et al., 2010). The advantages of PTTD lines are their broad bandwidth, high frequency operation and immunity to electromagnetic interference. In addition, fiber-based PTTD lines are readily compatible with fiber systems, robust, compact and lightweight, and they present low insertion loss.

Recently several types of fiber-based PTTD lines were proposed. For example, an optically controlled PTTD line based on stimulated Brillouin scattering demonstrates a fast time response within a relatively small range of the time delay (230 ps were reported using a fiber of 3.5 km length) (Zadok et al., 2007). Another example is the tunable PTTD line based on a uniform or chirped FBGs perturbed by heating or mechanical stress (Ortega et al., 2000; Liu et al., 2002; Perez-Millán et al., 2004), which permits simple experimental realization and easy tuning. However, such system has a very slow response (below 1 ms). In a number of PTTD lines tunable light sources are required to adjust the time delay (Liu et al., 2003; Blais et al., 2009), but this approach is not easily scalable when a large number of independent delays need to be adjusted.

Here we discuss a tunable PTTD line based on longitudinal ultra-sound modulation of a FBG written in a standard fiber similar to SMF-28. This device operates with a fixed optical carrier, demonstrates a wide time delay range (400 ps) and a fast response time [μs range, see Delgado-Pinar et al. (2006)].
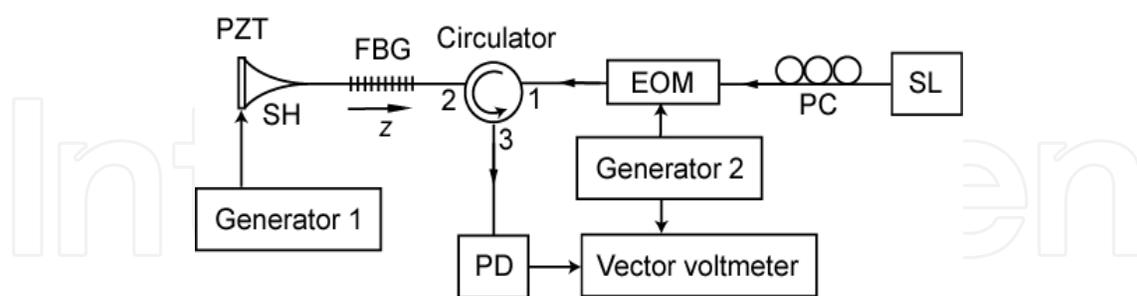

Fig. 25. Experimental setup. SL: semiconductor laser; PC: polarization controller; EOM: electro-optical amplitude modulator; FBG: fiber Bragg grating; PZT: piezoelectric transducer; SH: fused silica horn; PD: photodetector

The setup of the PTTD line is shown in Fig. 25. Light from a single-frequency semiconductor laser (SL) modulated by an electro-optical amplitude modulator (EOM) with a frequency of f_m = 400 MHz is sent through the optical circulator to a long uniform FBG written in a standard photosensitive fiber; the RF modulation depth is chosen to be comparatively low (~ 10%), which maintains a practically linear regime of light modulation. The FBG is 12 cm long, with a

Bragg wavelength of 1530.8 nm and reflectivity of 99.99% (40 dB transmission attenuation measured at the Bragg wavelength) that corresponds to a coupling coefficient $\kappa = 0.442$ cm^{-1}.

In the experimental arrangement, a longitudinal acoustic wave is generated by a piezoelectic (PZT) disk attached to a heat sink. This wave is launched along the single-mode optical fiber containing the uniform FBG using a fused silica horn (SH). The PZT is driven by Generator 1 at the PZT resonance frequency (2.08 MHz in our case). The light reflected by the FBG is registered by a photodetector connected to a vector voltmeter. AC voltage from Generator 2 drives the EOM; it is also used as a reference signal for the RF phase measurements.

The operation principle of such a PTTD line is based on the reflection of narrow-line light by one of the FBG side bands generated by the longitudinal acoustical wave. This wave modulates both the period and the refractive index of the grating producing thereby a sinusoidal chirp that moves along the fiber synchronously with the acoustic wave, and will be described by an effective phase modulation of the grating with amplitude $\Delta\Phi$. Under these conditions, the refractive index for the light mode propagating through the single-mode fiber core (so called LP_{01} mode) is written as follows:

$$
\begin{aligned}
n(z,t) &= n_0 + \Delta n \cos\left[Kz - \Delta\Phi\cos\left(k_s z + \Omega t\right)\right] = n_0 + \Delta n J_0(\Delta\Phi)\cos(Kz) \\
&+ 2\Delta n \cos(Kz)\sum_{m=1}^{\infty}(-1)^m J_{2m}(\Delta\Phi)\cos\left[2m\left(k_s z + \Omega t\right)\right] \\
&+ 2\Delta n \sin(Kz)\sum_{m=1}^{\infty}(-1)^{m-1} J_{2m-1}(\Delta\Phi)\cos\left[(2m-1)\left(k_s z + \Omega t\right)\right],
\end{aligned}
\tag{3}
$$

where n_0 is the effective refractive index for LP_{01} mode, Δn is the grating amplitude, $K = 2\pi/\Lambda$ is the unperturbed grating wavenumber (Λ is the grating period), z is the distance along the fiber, $\Delta\Phi$ is the phase modulation amplitude, k_s is the acoustic wavenumber, Ω is the angular acoustic frequency, m is a natural number corresponding to the order of the FBG side band, and J_m is the Bessel function of the m-th order. From Eq. 3 one can see that the longitudinal acoustic wave produces a series of the traveling FBGs with amplitudes depending on $\Delta\Phi$.

Using the coupled-wave theory (Erdogan, 1997), one can obtain the following set of the coupled-wave equations for two contra-propagating optical waves (one probe wave, $A_{\pm l}$, and one reflected wave, $B_{\pm l}$) falling into the $\pm l$ sideband induced by the acoustic wave and interacting with the perturbed grating described by Eq. 3:

$$
\frac{dA_{\pm l}}{dz} = -i\Delta\beta_{\pm l}A_{\pm l} + i^{(l-1)}\kappa_l B_{\pm l},
\tag{4}
$$

$$
\frac{dB_{\pm l}}{dz} = i\Delta\beta_{\pm l}B_{\pm l} + (-i)^{(l-1)}\kappa_l A_{\pm l},
\tag{5}
$$

where $\pm l$ is the sideband number, $\Delta\beta_{\pm l} = \beta - (\beta_0 \mp lk_s/2) = 2\pi n_0(\lambda^{-1} - \lambda_0^{-1}) \pm l\pi/\lambda_s$ is the detuning from the $\pm l$-sideband Bragg wavelength, λ_0 is the Bragg wavelength of the unperturbed FBG, λ is the probe light wavelength, β and β_0 are the light wavenumbers that correspond to λ and λ_0, and $\kappa_l = \kappa_0 J_l(\Delta\Phi)$ is the coupling coefficient for the l-th sideband (κ_0 is the coupling coefficient of the unperturbed FBG).

The analysis based on the theory developed by Barmenkov et al. (2006, 2010) permits one to write the equations for the sideband reflectivity, R_l, and the sideband effective length, $L_{\pm l}^{eff}$, in the following form:

$$R_{\pm l} = \left(\tanh \left(\kappa_{\pm l} L \right) \right)^2 , \tag{6}$$

$$L_{\pm l}^{eff} = \frac{1}{2\kappa_{\pm l}} \tanh \left(\kappa_{\pm l} L \right) = \frac{L\sqrt{R_{\pm l}}}{2\operatorname{atanh}\left(\sqrt{R_{\pm l}}\right)} , \tag{7}$$

where L is the FBG length. The formula for the group delay is found as

$$\tau_{\pm l} = 2 n_0 L_{\pm l}^{eff} / c . \tag{8}$$

From the last three equations one can conclude that the sideband diffraction efficiency, the effective length and the group delay may be controlled by the amplitude of the phase modulation of the grating induced by the acoustic wave, which, in turn, depends on the acoustic wave magnitude. The sideband Bragg wavelength can be tuned by adjusting the acoustical frequency within the PZT resonance in the case of a slight tuning, or by replacing the PZT with another one having the necessary resonance frequency.

The diffraction efficiency of the FBG sidebands can be measured using a wide-spectrum LED connected directly to the circulator port 1, and an optical spectrum analyzer (OSA) connected, in turn, to the port 3 instead of a photodetector (see Fig. 25); The Generator 2 is switched off. Fig. 26(a) shows the FBG spectra at different AC voltages applied to the PZT. At low voltages, the ±1 sidebands have amplitudes much higher than that of the high-order sidebands. Reflectivity of the ±1 sidebands did not reach 100% because the OSA resolution was not enough to resolve comparatively narrow reflection peaks (3 dB spectrum width is about 40 pm). Note that a proper FBG design based on the grating apodization and chirping should permit increasing the sideband width.

As it is seen from Fig. 26 (b), the dependence of the +1 sideband efficiency on the voltage applied to the PZT is in good agreement with Eq. (6), assuming that the amplitude of the phase modulation of the grating is proportional to the PZT voltage; a slight difference observed at high voltage amplitudes (> 4V) could be explained by a small heating of the PZT, which slightly changes the PZT electromechanical coupling factor. Note that the ±1 sideband allows operation of AOSLM at low PZT voltages in comparison with high-order sidebands, the −1 sideband has the same properties as the +1 sideband.

The RF modulation envelope phase, Ψ_{+1}, is related directly to the +1 sideband group delay τ_{+1} and the effective length L_{+1}^{eff}:

$$\Psi_{+1} = 2\pi\tau_{+1} f_m = 4\pi n_0 L_{+1}^{eff} f_m / c \tag{9}$$

Thus, the dependence of Ψ_{+1} on +1 sideband efficiency is the basic feature that permits to implement a dynamic control of the group delay and the effective length of the grating by means of the AC voltage. The same is for the −1 sideband.

Fig. 27(a) shows the experimental relationship between Ψ_{+1} and the amplitude of the AC voltage applied to the PZT. One can see that the phase decreases as voltage amplitude increases, which is explained by decreasing of the group delay and the effective length. Figure 27(b) plots these two parameters versus the +1 sideband diffraction efficiency. The experimental data show a good agreement with Eqs. (7) and (8). Since the optical path between the EOM and the photodetector was relatively long (the fiber length was ~ 2 m), producing an additional phase shift into the measured Ψ_{+1} values, the experimental data were corrected by a phase offset (the right scale in Fig. 27(a) that permits to compensate the

fiber length excess. The correcting parameter was chosen so that the +1 sideband effective length is equal to a half of FBG physical length at low sideband efficiency (low PZT voltage), as the Eq. (7) predicts.
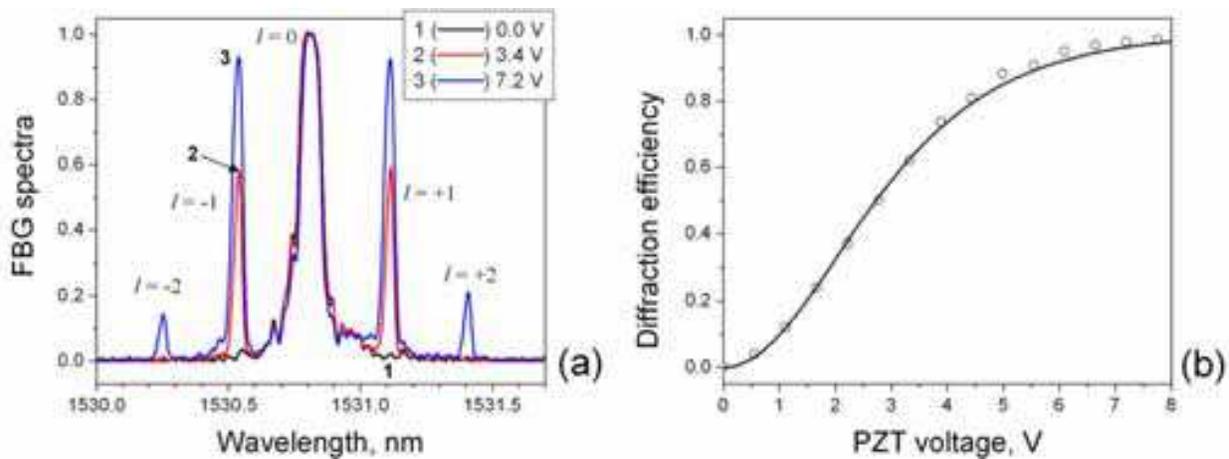

Fig. 26. (a) Spectra of FBG perturbed by ultra-sound wave at different PZT voltages (the voltage values are shown in the upper right corner); l indicates the sideband number. The OSA resolution is 20 pm. (b) Dependence of the +1 sideband efficiency on PZT voltage. Circles: experimental data; solid line: fitting

From Fig. 27(b) one can conclude that the group delay and the effective length for the +1 sideband depend on its efficiency that is controlled electrically by the AC voltage applied to the PZT. In the experiments, the group delay was adjustable from 150 ps to 550 ps, i.e., covering a range of 400 ps. Within the 3 dB range of the sideband efficiency, the group delay could be continuously adjusted from 150 to 450 ps (a range of 300 ps). The implementation of an automatic SL power control would permit to adjust the group delay at constant optical power, compensating for the reflectivity changes of the sideband. The response time of this PTTD line is approximately 20 μs and is determined by the acoustic wave speed and the grating length.
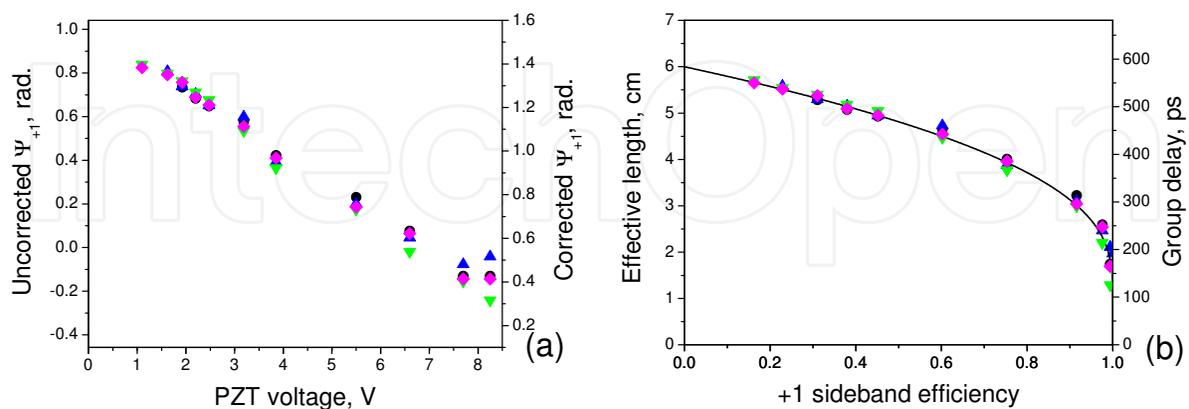
Fig. 27. (a) Dependence of the RF modulation envelope phase of light reflected from the FBG +1 sideband on amplitude of voltage applied to PZT. The left scale: uncorrected values, the right scale: corrected values. (b) FBG +1 sideband effective length and group delay versus the diffraction efficiency. Symbols: experimental data; solid line: curve calculated by Eq. (7). In both figures different symbols correspond to different experimental series

In summary, the experimental and theoretical study of the phase and group delay response of a FBG modulated by a longitudinal acoustic wave permits the implementation of electrically-tuned PTTD line controlled by the AC voltage applied to the piezo-electric transducer that generates the acoustic wave. The proposed PTTD line permits to vary the group delay in the range of 400 ps.

3.4 *Q*-switching in a distributed feedback fiber laser

When the acoustic perturbation is not a harmonic wave but a single pulse, its passage through the FBG creates a defect which can be used to control the *Q*-factor in a DFB all-fiber laser. Single-mode narrow-linewidth lasers are of great interest as they have a wide applicability in fields such as high-resolution interferometry, distributed Brillouin sensing, optical coherent communications, etc. DFB lasers based on semiconductor technology have linewidths typically in the MHz domain; due to the short cavity length and low thermal dissipation its output spectrum is typically broad. Fiber lasers usually operate in a multi-mode regime and have a broad spectrum; to make efficient single-mode narrow-linewidth fiber lasers different approaches have been implemented. Fiber rings lasers fulfill the requirement and produce narrow-linewidth outputs; most importantly, they can be made widely tunable. However, they are more complex and –because of their long cavities– susceptible to mode hopping. Distributed Bragg reflector (DBR) fiber lasers is another option, however, temperature stabilization is still required to prevent mode hopping and, in the short laser cavity, the pump wave absorption is low, as a consequence the DBR fiber laser is not efficient and external optical amplifiers are generally needed (Babin et al., 2007). Distributed feedback fiber lasers can overcome part of these problems. They have the simplest, robust and compact design providing operation without mode hopping. Its fabrication is relatively simple, and involves the writing of a grating structure –i.e. a fiber Bragg grating– with ultraviolet light into an active fiber. Single-mode pump leads to an alignment free resonator with optimum overlap of pump and signal light. For these FBG-based DFB lasers, the distributed reflection occurs in the grating when a phase shift has been generated within it. A number of techniques have been proposed for this; however, statics phase shifts only allow CW operation, which translates into low power emission. Recently, some approaches have been reported to obtain single-frequency pulsed all-fiber lasers, based on active *Q*-switching of DFB fiber cavities. The pulsed operation of a DFB laser is interesting because for certain applications (e.g. Brillouin sensing), it is not only required a narrow linewidth but also a peak power about a minimum threshold, which otherwise could not be reached by a CW operation (Cuadrado-Laborde et al., 2008).

Figure 28(a) shows the scheme of the proposed DFB all-fiber laser. The FBG was 100 mm long, and was written in a 1500 ppm erbium hydrogen-loaded fiber (codoped with germanium and aluminum) of the same length using a doubled argon laser and a uniform period mask. The FBG shows more than 30 dB attenuation at the Bragg wavelength of 1532.45 nm and a 3 dB bandwidth of 88 pm. The FBG was pumped through a 980/1550 nm WDM with a 980 nm semiconductor laser, providing a maximum pump power of 130 mW. A square shape rod of a magnetostrictive material (Terfenol-D, 15 mm long and 1 mm² section) was bonded outside the FBG to a free section of fiber at 88 mm from the center of the grating, and placed inside a small coil, see Fig. 28(a).

The acoustic pulse generated by using a magnetostrictive device has a superior performance as compared with piezoelectric devices which have a frequency-dependent response

characterized by strong mechanical resonances. On the contrary, a magnetostrictive device has a lower frequency range but its frequency response is basically flat. The magnetostrictive rod can be bonded directly over the FBG, but this has some detrimental consequences. First, any external actuator bonded directly on the fiber is likely to exhibit long-term instabilities (Andrés et al., 2008). Second, once the magnetostrictive rod is fixed to the fiber, any temperature change generates a differential expansion between the fiber and the magnetostrictive rod, producing a local static perturbation of the FBG that may cause CW emission. Because of this, we avoided these drawbacks by attaching he magnetostrictive rod outside the FBG and generating a dynamic defect in the FBG through an acoustic axially-propagating pulse. Thereby, when a pulse of electric current is applied to the coil, the small rod lengthens and stretches the section of fiber attached to it, generating in this way a longitudinal acoustic pulse that propagates toward the FBG. The pulse propagating along the grating generates a phase shift opening a transmission peak within the reflection band of the grating; as a consequence a high Q resonance is produced and a laser pulse is emitted (Pérez-Millán et al., 2005b; Delgado-Pinar et al., 2007). Otherwise, if no perturbation is present within the FBG, there is no efficient feedback for the optical signal, and the laser emission is not allowed. Since the defect is not fixed, but induced by a travelling acoustic pulse with a time-varying position along the FGB, one could think that this might have important consequences on the spectral position of the transmission peak. However, this is not the case, as it was recently demonstrated (Andrés et al., 2008). The spectral position of the resonance is constant, no matter the actual spatial location of the acoustic pulse, although some short transients are produced when the pulse overlaps the extremes of the FBG. This property insures that the laser will emit with a narrow linewidth, preserving one of the most attractive properties of DFB fiber lasers. The transmission properties of the passive FBG –i.e. without pumping– interacting with the acoustic pulses were investigated by illuminating the FBG with a tunable laser at the Bragg wavelength and detecting the reflected signal. When the coil current is zero, the reflectance is maximal; but when a current pulse of 220 mA and 5 μs temporal width is applied to the coil, a transmission peak opens the reflection band, being as narrow as 2 μs (FWHM), see Fig. 28(b). Figures 29(a) to 29(c) shows the voltage pulses applied to the current driver, the backward output train of the DFB laser, a detail of the optical pulse, and a single current pulse applied to the coil, respectively. The observed delay time between the voltage signal and the optical pulses is mainly due to the distance that pulses have to travel from the magnetostrictive device to the FBG, see Fig. 28(a).
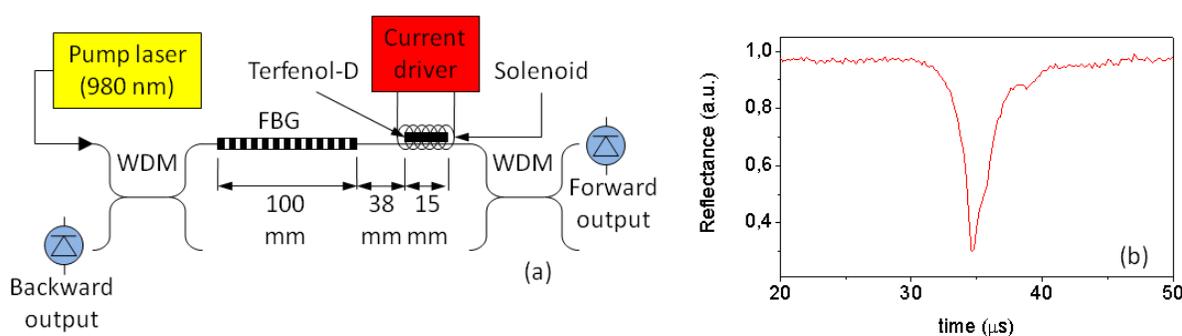

Fig. 28. (a) Q-switched distributed feedback-fiber laser setup. (b) Reflection at the Bragg wavelength when an acoustic pulse travels along the FBG
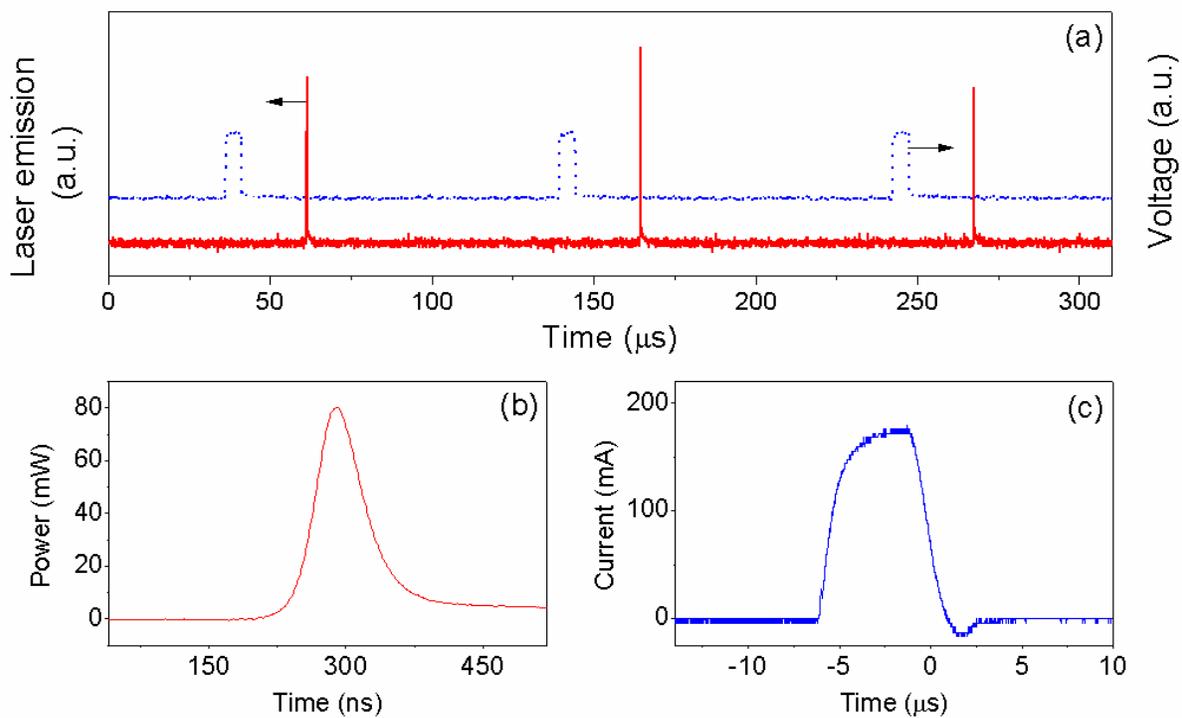
Fig. 29. *Q*-switched DFB behavior at 10 kHz repetition rate and 80 mW of pump power. (a) Emitted optical train pulses and voltage signal applied to the current driver, (b) detail of a single optical pulse of the train, and (c) detail of a single current pulse applied to the coil
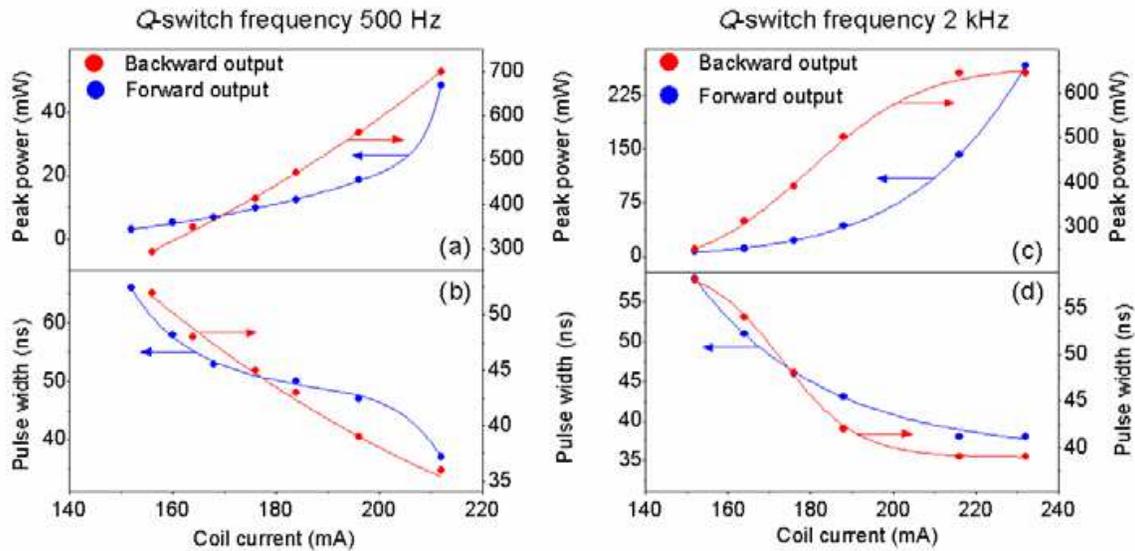

Fig. 30. Peak power and pulse width for backward and forward outputs as a function of the coil current for two different *Q*-switched repetition rates: 500 Hz (a, b) and 2 kHz (c, d), respectively, and 55mW of pump power

One key characteristic in this setup is its versatility, which is given by the possibility of selecting a variety of peak powers and time widths just by varying the coil current. Figure 30 shows the peak power and pulse width for backward and forward outputs as a function of the coil current for two different repetition rates: 500 Hz and 2 kHz, Figs. 30(a-b) and 30(c-

d), respectively. There is a low threshold value for the coil current (I), bellow this value; there is not laser emission, since the *Q* value is not high enough (i.e. I < 150 mA). Above this value, the laser emission is allowed and one optical pulse per cycle is emitted; at higher electric currents (i.e., I > 230 mA) there are two optical pulses per current pulse. At different repetition rates the peak power and time width values change but the general trend is preserved. The effect of pump power on the optical pulses, for repetition rates ranging from 200 Hz to 20 kHz, is shown in Figs. 31(a,b) and 31(c,d), for the backward and forward outputs, respectively. A fixed coil current of 200 mA amplitude was used in all cases. At each different frequency, there is a corresponding pump power threshold. Above threshold, the peak power increases with pump power and there is a corresponding reduction of the pulse width. Pulses of 800 mW peak power and 32 ns time width were obtained at 500 Hz repetition rate and 46 mW pump power for the backward output. If pump power is high enough, the laser emits more than one pulse per cycle, defining in this way an upper limit also. It can be observed the differences in peak powers between backward and forward outputs, being higher in the first case. Temporal widths and peak power jitters were measured to be below 5 %.
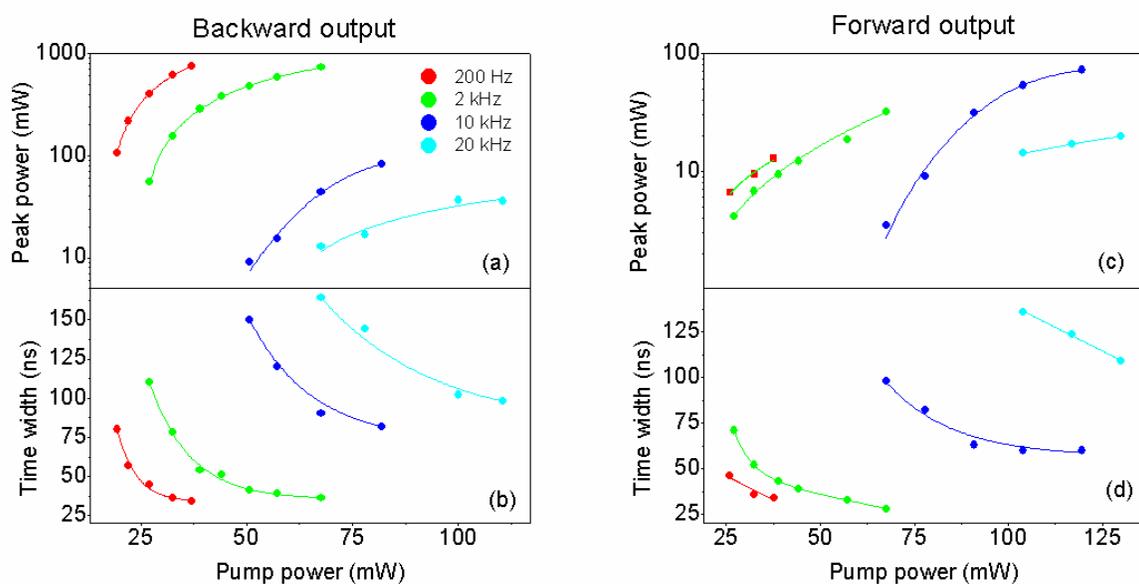

Fig. 31. Peak power and pulse width for the backward (a, b) and forward (c, d) laser outputs, as a function of the pump power, for several repetition rates

The emission linewidth was measured, using a classical heterodyne configuration (Galtarossa et al., 1993). A tunable laser was used as local oscillator with spectral linewidth of 100 kHz. The output of this laser was superimposed to the optical pulses of the DFB laser (backward output), through a 1550 nm 20 dB coupler. The beat signal at the coupler output was detected with a 1 GHz bandwidth photodetector, and analyzed with a 500 MHz bandwidth oscilloscope. From the spectrum of the beating signals, resulted a DFB laser linewidth of 6 MHz. The optical pulses from the DFB all-fiber laser had a temporal width of 80 ns, so according to the time-frequency uncertainty principle (Agrawal, 2001), its bandwidth cannot be lower than 5.5 MHz. From the comparison between this last value and the linewidth measurement, we conclude that the optical pulses of our DFB fiber laser are transform-limited. Finally, as an example of application of this compact laser source, we demonstrate the possibility to generate Brillouin scattering for sensing purposes. Brillouin scattering

essentially refers to the scattering of a light wave by an acoustic wave (Agrawal, 2001). When a coherent pulse of light propagates through a medium, part of its energy is backscattered due to a non elastic interaction with the acoustic phonons. This back-scattered light is composed of a frequency down-shifted Stokes light and an up-shifted anti-Stokes light, whose spectral positions are dependent on temperature and strain of the fiber, in this way allowing its use as a sensing mechanism (Culverhouse et al., 1989a, 1989b; Bao et al., 1995; Parker et al., 1998; Y. Li et al., 2003). Figure 32(b) shows the backscattered light spectrum after illuminating a 10.5 km length optical fiber spool (Corning SMF-28) with the backward output of our DFB all-fiber laser (4 kHz repetition rate and 74 mW pump power). The Brillouin spectrum was registered with an optical spectral analyzer (resolution of 20 pm). The extreme of the fiber optic spool was terminated with a matching refractive index liquid (n = 1.46). The central (highest) peak corresponds to the proper laser beam reflections after successive connections and splices together with Rayleigh scattering. Peaks symmetrically positioned at both sides correspond to the Brillouin backscattering by Stokes and anti-Stokes processes (Parker et al., 1998). The measured Brillouin shift results in 88 pm (i.e. 11.24 GHz at 1532.4 nm), which correspond to the expected value in this fiber (Agrawal, 2001). Fiber optics distributed temperature, and/or strain, sensors have becoming very attractive for applications requiring sensing lengths of many kilometers, principally due to its inexpensiveness and availability. Optical fiber based distributed sensor systems normally make use of the principle of optical time domain reflectometry (Parker et al., 1998). Therefore, an optical pulse is launched into one end of the fiber system and the variation of the scattered light is detected as a function of time, giving in this way information of temperature or strain as a function of distance. A key requirement in this measurement system is a stable light source with a narrow enough spectral linewidth. In addition, for time domain reflectometry applications, the sensor spatial resolution proportionally depends on the optical pulse width, so it must be considered also. In order to fulfill all these requirements, solid state lasers with external cavities –plus amplifiers and amplitude modulators– are currently used in these systems (Parker et al., 1998). Here we propose using this compact all-fiber pulsed light source as a relatively simpler alternative.
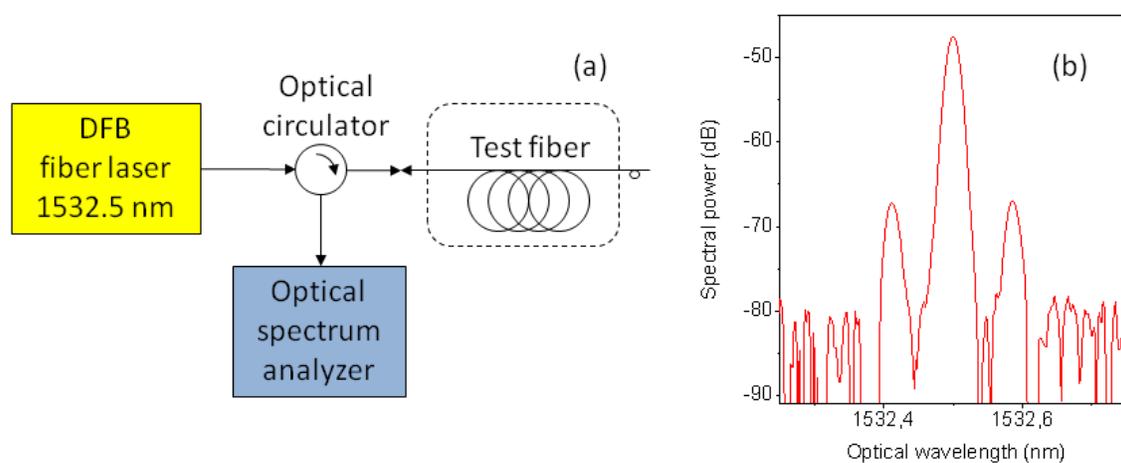

Fig. 32. Schematic diagram of the setup used for the Brillouin backscattering measurements. Brillouin spectra at room temperature for a 10.5-km length Corning SMF-28 optical fiber spool, for a backward output at 4 kHz repetition rate and 74 mW pump power

4. Conclusions

In this chapter we have discussed the use of acoustic waves to control all-fiber devices for different applications. In Section 2 we focused on novel applications of acousto-optic fiber devices based on flexural acoustic waves. As an example of application, we described in subsection 2.1 an actively Q-switched ytterbium-doped strictly all-fiber laser. Q-switching modulation was achieved by intermodal modulation induced by flexural acoustic waves travelling in a tapered optical fiber. Q-switched light pulses at 1064.1 nm were successfully obtained at repetition rates in the range 1-10 kHz, with pump powers between 59 mW and 88 mW. Best results were for laser pulses of 118 mW peak power, 1.8 µs of time width, with a pump power of 79 mW, at 7 kHz repetition rate.

Next, in subsection 2.2 we described an actively mode-locked fiber ring laser. As mode-locker was proposed an acousto-optic modulator driven by standing flexural acoustic waves, which couples core-to-cladding modes in a standard single-mode optical fiber. Among the remarkable features of the modulator, we mention its high modulation depth (72%), broad bandwidth (187 GHz), easy tunability in the optical wavelength, and low insertion losses (0.7 dB). The narrowest optical pulses obtained were of 95 ps time width, 21 mW peak power, repetition rate of 4.758 MHz, and 110 mW of pump power. We also characterized this laser as a function of the RF voltage that controls the modulator, the length of the active fiber, and the optical bandwidth of an intracavity filter implemented with a fiber Bragg grating. Best results were for output light pulses of 34 ps time width, and 1.4 W peak power.

In Section 3 we focused on novel applications of acousto-optic devices based on the interaction of longitudinal acoustic waves with fiber Bragg gratings. From the comparison of the acoustic wavelength with the periodicity of the FBG, two well-different situations could be distinguished: the long-wavelength and the short-wavelength regimes. As an example of application of the former, we described in subsection 3.1 an in-fiber resonant acousto-optic modulator suitable for Q-switching applications. The modulator consists of a short-length FBG modulated by a long-wavelength standing longitudinal acoustic wave. The acoustic wave shifts periodically in time the reflection band of the grating along a given wavelength range; by using this modulator, we demonstrated an actively Q-switched all-fiber laser. Output light pulses of 1.6 W peak power and 172 ns time width were obtained at 18 kHz repetition rate.

Next, in section 3.2 and 3.3 we focused on applications of acousto-optic devices based on the interaction of longitudinal acoustic waves with fiber Bragg gratings in the short-wavelength regime. Thus, in subsection 3.2 we proposed the use of an acousto-optic supper-lattice modulator as mode-locker. Since an acousto-optic supper-lattice modulator can be driven in two different ways either by standing or traveling acoustic waves; we discussed first the construction of a mode-locked laser driven by standing acoustic waves. In this configuration we obtained transform-limited optical light pulses of up to 120 mW peak power and 780 ps pulse width generated at a fixed repetition rate of 9 MHz, with an emission linewidth of 2.8 pm at 1530.5 nm. We also study the influence of different parameters on the mode-locking process such as: frequency detuning, EDF length, amplitude modulation, and dispersion. In this case, narrower pulses were obtained at higher modulation depths, normal dispersion, and shorter lengths of active fiber. Best results were reached when the laser was optimized according to these variables (160mW peak power and 630 ps pulse width). On the other hand, we showed that by slightly modifying the cavity, it is possible to operate the laser in a double-active Q-switching mode-locking regime. It is worth to mention that this approach was unique, being this double-active all-fiber laser the first of its kind. To this end, we attached a magnetostrictive rod to the output FBG to modulate the Q factor of the Fabry–

Perot cavity. Fully modulated *Q*-switched mode-locked trains of optical pulses were obtained for a wide range of pump powers and repetition rates. For a *Q*-switched repetition rate of 500 Hz and a pump power of 100 mW, the laser generates trains of 12–14 modelocked pulses of about 1 ns each, within an envelope of 550 ns, an overall energy of 0.65 μJ, and a peak power higher than 250 W for the central pulses of the train. Then, we discussed the construction of a mode-locked laser when the mode-locker is driven by travelling acoustic waves. In this case, the modulation frequency is half the frequency obtained when standing acoustic waves are used. Optical pulses were obtained of 530 mW peak power, 700 ps pulse width, at a repetition rate of 4.1 MHz. The variation of the pulses parameters under frequency detuning and applied voltage was also studied. Finally, we demonstrated that it is not necessary to modify the setup in order to reach double active *Q*-switching and mode-locking, when travelling acoustic waves were used to drive the mode-locker. In this case the commutation between mode-locking and *Q*-switching mode-locking is remarkably simple; it just needs use of a different electrical signal to drive the piezoelectric of the mode-locker, i.e. from a sinusoidal to a burst-sinusoidal electrical signal. In this case, fully modulated 10–25 modelocked pulses around 700 ps each within a *Q*-switching envelope around 1 μs and a maximum overall energy of 0.68 μJ were obtained.

In subsection 3.3 we shown another example of application of acousto-optic devices based on the interaction of longitudinal acoustic waves with fiber Bragg gratings in the short-wavelength regime. Thus, we carried out an experimental and theoretical study of the phase and group delay response of the acousto-optic supper-lattice modulator. The phase properties of the first sidebands permit the implementation of electrically-tuned photonic true-time delay line controlled by the AC voltage applied to the piezoelectric transducer that generates the acoustic wave. The proposed photonic true-time delay line permits to vary the group delay up to 400 ps.

Finally, when the acoustic perturbation is not a harmonic wave but a single pulse, its passage through the FBG creates a defect which can be used to control the *Q*-factor in a DFB all-fiber laser, subsection 3.4. Thus, we shown a single-mode, transform-limited, actively *Q*-switched distributed-feedback fiber laser. Optical pulses of 800 mW peak power, 32 ns temporal width, and up to 20 kHz repetition rates were obtained. The measured linewidth demonstrates that these pulses are transform limited: 6 MHz for a train of pulses of 10 kHz repetition rate, 80 ns temporal width, and 60 mW peak power. Efficient excitation of spontaneous Brillouin scattering was demonstrated.

In summary, photonic devices can benefit highly of a strictly all-fiber configuration which provides them a series of attractive advantages. Among all the proposed in-fiber solutions, devices controlled by acoustic waves have been by far the most employed, especially in mode-locked lasers, providing a broad range of alternatives. The recent advances in acoustically controlled photonic systems positioned them as a promising candidate for commercially available systems in the near future.

5. Acknowledgments

## 6. References

Agrawal, G. P. (2001). *Nonlinear Fiber Optics*, Academic Press, New York, 2001.

Álvarez-Chávez, J. A.; Offerhaus, H. L.; Nilsson, J.; Turner, P. W.; Clarkson, W. A.; Richardson, D. J. (2000). High-energy, high-power ytterbium-doped Q-switched fiber laser. *Optics Letters*, 25 (1): 37-39 Jan 1 2000.

Andersen, T. V.; Pérez-Millán, P.; Keiding, S. R.; Agger, S.; Duchowicz, R.; Andrés, M. V. (2006). All-fiber actively Q-switched Yb-doped laser. *Optics Communications*, 260 (1): 251-256 Apr 1 2006.

Andres, M. V.; Cruz, J. L.; Díez, A.; Pérez-Millán, P.; Delgado-Pinar, M. (2008). Actively Q-switched all-fiber lasers. *Laser Physics Letters*, 5 (2): 93-99 Feb 2008.

Babin, S. A.; Churkin, D. V.; Ismagulov, A. E.; Kablukov, S. I.; Nikulin, M. A. (2007). Single frequency single polarization DFB fiber laser. *Laser Physics Letters*, 4 (6): 428-432 Jun 2007.

Bao, X.; Dhliwayo, J.; Heron, N.; Webb, D. J.; Jackson, D. A. (1995). Experimental and theoretical-studies on a distributed temperature sensor-based on Brillouin-scattering. *Journal of Lightwave Technology*, 13 (7): 1340-1348 Jul 1995.

Barmenkov, Y. O.; Zalvidea, D.; Torres-Peiró, S.; Cruz, J. L.; Andrés, M. V. (2006). Effective length of short Fabry-Perot cavity formed by uniform fiber Bragg gratings. *Optics Express*, 14 (14): 6394-6399 Jul 10 2006.

Barmenkov, Y. O.; Cruz, J. L.; Díez, A.; Andrés, M. V. (2010). Electrically tunable photonic true-time-delay line. *Optics Express*, 18 (17): 17859-17864 Aug 16 2010.

Belanger, P. A. (2005). On the profile of pulses generated by fiber lasers. *Optics Express*, 13 (20): 8089-8096 Oct 3 2005.

Bello-Jiménez, M.; Cuadrado-Laborde, C.; Sáez-Rodriguez, D.; Díez, A.; Cruz, J. L.; Andrés, M. V. (2010). Actively mode-locked fiber ring laser by intermodal acousto-optic modulation. *Optics Letters*, 35 (22): 3781-3783 Nov 15 2010.

Bello-Jiménez, M.; Cuadrado-Laborde, C.; Díez, A.; Cruz, J. L.; Andrés, M. V. (2011). Experimental study of an actively mode-locked fiber ring laser based on in-fiber amplitude modulation. *Applied Physics B*, in press (2011).

Birks, T. A.; Russell, P. S. J.; Pannell, C. N. (1994). Low-power acoustooptic device based on a tapered single-mode fiber. *IEEE Photonics Technology Letters*, 6 (6): 725-727 Jun 1994.

Blais, S.; Yao, J. P. (2009). Photonic true-time delay beamforming based on superstructured fiber Bragg gratings with linearly increasing equivalent chirps. *Journal of Lightwave Technology*, 27 (9): 1147-1154 May 1 2009.

Bonadeo, N. H.; Knox, W. H.; Roth, J. M.; Bergman, K. (2000). Passive harmonic mode-locked soliton fiber laser stabilized by an optically pumped saturable Bragg reflector. *Optics Letters*, 25 (19): 1421-1423 Oct 1 2000.

Capmany, J.; Ortega, B.; Pastor, D.; Sales, S. (2005). Discrete-time optical processing of microwave signals. *Journal of Lightwave Technology*, 23 (2): 702-723 Feb 2005.

Caucheteur, C.; Mussot, A.; Bette, S.; Kudlinski, A.; Douay, M.; Louvergneaux, E.; Megret, P.; Taki, M.; Gonzalez-Herraez, M. (2010). All-fiber tunable optical delay line. *Optics Express*, 18 (3): 3093-3100 Feb 1 2010.

Costantini, D. M.; Limberger, H. G.; Lasser, T.; Muller, C. A. P.; Zellmer, H.; Riedel, P.; Tunnermann, A. (2000). Actively mode-locked visible upconversion fiber laser. *Optics Letters*, 25 (19): 1445-1447 Oct 1 2000.

Cuadrado-Laborde, C.; Delgado-Pinar, M.; Torres-Peiró, S.; Díez, A.; Andrés, M. V. (2007). Q-switched all-fibre laser using a fibre-optic resonant acousto-optic modulator. *Optics Communications*, 274 (2): 407-411 Jun 15 2007.

Cuadrado-Laborde, C.; Perez-Millán, P.; Andres, M. V.; Díez, A.; Cruz, J. L.; Barmenkov, Y. O. (2008). Transform-limited pulses generated by an actively Q-switched distributed fiber laser. *Optics Letters*, 33 (22): 2590-2592 Nov 15 2008.

Cuadrado-Laborde, C.; Díez, A.; Delgado-Pinar, M.; Cruz, J. L.; Andres, M. V. (2009a). Mode locking of an all-fiber laser by acousto-optic superlattice modulation. *Optics Letters*, 34 (7): 1111-1113 Apr 1 2009.

Cuadrado-Laborde, C.; Diez, A.; Cruz, J. L.; Andres, M. V. (2009b). Doubly active Q switching and mode locking of an all-fiber laser. *Optics Letters*, 34 (18): 2709-2711 Sep 15 2009.

Cuadrado-Laborde, C.; Diez, A.; Cruz, J. L.; Andres, M. V. (2010a). Experimental study of an all-fiber laser actively mode-locked by standing-wave acousto-optic modulation. *Applied Physics B-Lasers and Optics*, 99 (1-2): 95-99 Apr 2010.

Cuadrado-Laborde, C.; Diez, A.; Cruz, J. L.; Andres, M. V. (2010b). Actively Q-switched and modelocked all-fiber lasers. *Laser Physics Letters*, 7 (12): 870-875 Dec 2010.

Culverhouse, D. O.; Farahi, F.; Pannell, C. N.; Jackson, D. A. (1989a). Potential of stimulated Brillouin-scattering as sensing mechanism for distributed temperature sensors. *Electronics Letters*, 25 (14): 913-915 Jul 6 1989.

Culverhouse, D. O.; Farahi, F.; Pannell, C. N.; Jackson, D. A. (1989b). Stimulated Brillouin-scattering - a means to realize tunable microwave generator or distributed temperature sensor. *Electronics Letters*, 25 (14): 915-916 Jul 6 1989.

Culverhouse, D. O.; Richardson, D. J.; Birks, T. A.; Russell, P. S. J. (1995). All-fiber sliding-frequency Er^{3+}/Yb^{3+} soliton laser. *Optics Letters*, 20 (23): 2381-2383 Dec 1 1995.

Delgado-Pinar, M.; Zalvidea, D.; Diez, A.; Perez-Millan, P.; Andres, M. V. (2006). Q-switching of an all-fiber laser by acousto-optic modulation of a fiber Bragg grating. *Optics Express*, 14 (3): 1106-1112 Feb 6 2006.

Delgado-Pinar, M.; Diez, A.; Cruz, J. L.; Andres, M. V. (2007). Single-frequency active Q-switched distributed fiber laser using acoustic waves. *Applied Physics Letters*, 90 (17): Art. No. 171110 Apr 23 2007.

Erdogan, T. (1997). Fiber crating spectra. *Journal of Lightwave Technology*, 15 (8): 1277-1294 Aug 1997.

French, P. M. W. (1995). The generation of ultrashort laser pulses. *Reports on Progress in Physics* 58 (2): 169-267 Feb 1995.

Galtarossa, A.; Nava, E.; Valentini, G. (1993). *Single-Mode Optical Fiber Measurement: Characterization and Sensing*, Ed. G. Cancellieri, Artech Pub. 1993.

Geister, G.; Ulrich, R. (1988). Neodymium-fiber laser with integrated-optic mode locker. *Optics Communications*, 68 (3): 187-189 Oct 1 1988.

Haus, H. A. (2000). Mode-locking of lasers. *IEEE Journal of Selected Topics in Quantum Electronics*, 6 (6): 1173-1185 Nov-Dec 2000.

Huang, D. W.; Liu, W. F.; Yang, C. C. (2000). Q-switched all-fiber laser with an acoustically modulated fiber attenuator. *IEEE Photonics Technology Letters*, 12 (9): 1153-1155 Sep 2000.

Hudson, D. D.; Holman, K. W.; Jones, R. J.; Cundiff, S. T.; Ye, J.; Jones, D. J. (2005). Mode-locked fiber laser frequency-controlled with an intracavity electro-optic modulator. *Optics Letters*, 30 (21): 2948-2950 Nov 1 2005.

Imai, T.; Komukai, T.; Yamamoto, T.; Nakazawa, M. (1997). A wavelength tunable Q-switched fiber laser using fiber Bragg gratings. *Electronics and Communications in Japan Part II-Electronics*, 80 (11): 12-21 Nov 1997.

Italia, V.; Pisco, M.; Campopiano, S.; Cusano, A.; Cutolo, A. (2005). Chirped fiber Bragg gratings for electrically tunable time delay lines. *IEEE Journal of Selected Topics in Quantum Electronics*, 11 (2): 408-416 Mar-Apr 2005.

Jeon, M. Y.; Lee, H. K.; Kim, K. H.; Lee, E. H.; Oh, W. Y.; Kim, B. Y.; Lee, H. W.; Koh, Y. W. (1998). Harmonically mode-locked fiber laser with an acousto-optic modulator in a Sagnac loop and Faraday rotating mirror cavity. *Optics Communications*, 149 (4-6): 312-316 Apr 15 1998.

Kee, H. H.; Lees, G. P.; Newson, T. P. (1998). Narrow linewidth CW and Q-switched erbium-doped fibre loop laser. *Electronics Letters*, 34 (13): 1318-1319 Jun 25 1998.

Kim, B. Y.; Blake, J. N.; Engan, H. E.; Shaw, H. J. (1986). All-fiber acoustooptic frequency shifter. *Optics Letters*, 11 (6): 389-391 Jun 1986.

Kim, H. S.; Yun, S. H.; Kwang, I. K.; Kim, B. Y. (1997). All-fiber acousto-optic tunable notch filter with electronically controllable spectral profile. *Optics Letters*, 22 (19): 1476-1478 Oct 1 1997.

Kuizenga, D. J.; Siegman, A. E. (1970). FM and AM mode locking of homogeneous laser .1. Theory. *IEEE Journal of Quantum Electronics*, QE 6 (11): 694-& 1970.

Li, Y. H.; Lou, C. Y.; Han, M.; Gao, Y. Z. (2001). Detuning characteristics of the AM mode-locked fiber laser. *Optical and Quantum Electronics*, 33 (6): 589-597 Jun 2001.

Li, Y. Q.; Zhang, F. C.; Yoshino, T. (2003). Wide-range temperature dependence of Brillouin shift in a dispersion-shifted fiber and its annealing effect. *Journal of Lightwave Technology*, 21 (7): 1663-1667 Jul 2003.

Li, X. W.; Peng, L. M.; Wang, S. B.; Kim, Y. C.; Chen, J. P. (2007). A novel kind of programmable 3(n) feed-forward optical fiber true delay line based on SOA. *Optics Express*, 15 (25): 16760-16766 Dec 10 2007.

Liu, W. F.; Russell, P. S. J.; Dong, L. (1997). Acousto-optic superlattice modulator using a fiber Bragg grating. *Optics Letters*, 22 (19): 1515-1517 Oct 1 1997.

Liu, W. F.; Russell, P. S. J.; Dong, L. (1998). 100% efficient narrow-band acoustooptic tunable reflector using fiber Bragg grating. *Journal of Lightwave Technology*, 16 (11): 2006-2009 Nov 1998.

Liu, Y. Q.; Yang, J. L.; Yao, J. P. (2002). Continuous true-time-delay beamforming for phased array antenna using a tunable chirped fiber grating delay line. IEEE *Photonics Technology Letters*, 14 (8): 1172-1174 Aug 2002.

Liu, Y. Q.; Yao, J. P.; Yang, J. L. (2003). Wideband true-time-delay beam former that employs a tunable chirped fiber grating prism. *Applied Optics*, 42 (13): 2273-2277 May 1 2003.

Myren, N.; Margulis, W. (2005). All-fiber electrooptical mode-locking and tuning. *IEEE Photonics Technology Letters*, 17 (10): 2047-2049 Oct 2005.

Ortega, B.; Cruz, J. L.; Capmany, J.; Andres, M. V.; Pastor, D. (2000). Analysis of a microwave time delay line based on a perturbed uniform fiber Bragg grating operating at constant wavelength. *Journal of Lightwave Technology*, 18 (3): 430-436 Mar 2000.

Parker, T. R.; Farhadiroushan, M.; Feced, R.; Handerek, V. A.; Rogers, A. J. (1998). Simultaneous distributed measurement of strain and temperature from noise-initiated Brillouin scattering in optical fibers. *IEEE Journal of Quantum Electronics*, 34 (4): 645-659 Apr 1998.

Pérez-Millán, P.; Torres-Peiró, S.; Mora, J.; Díez, A.; Cruz, J. L.; Andres, M. V. (2004). Electronic tuning of delay lines based on chirped fiber gratings for phased arrays powered by a single optical carrier. *Optics Communications*, 238 (4-6): 277-280 Aug 15 2004.

Pérez-Millán, P.; Díez, A.; Andres, M. V.; Zalvidea, D.; Duchowicz, R. (2005a). Q-switched all-fiber laser based on magnetostriction modulation of a Bragg grating. *Optics Express*, 13 (13): 5046-5051 Jun 27 2005.

Pérez-Millán, P.; Cruz, J. L.; Andres, M. V. (2005b). Active Q-switched distributed feedback erbium-doped fiber lasers. *Applied Physics Letters*, 87 (1): Art. No. 011104 Jul 4 2005.

Philippov, V. N.; Kiryanov, A. V.; Unger, S. (2004). Advanced configuration of erbium fiber passively Q-switched laser with Co^{2+}: ZnSe saturable absorber. *Ieee Photonics Technology Letters*, 16 (1): 57-59 Jan 2004.

Phillips, M. W.; Ferguson, A. I.; Hanna, D. C. (1989a). Frequency-modulation mode-locking of a Nd^{3+}-doped fiber laser. *Optics Letters*, 14 (4): 219-221 Feb 15 1989.

Phillips, M. W.; Ferguson, A. I.; Kino, G. S.; Patterson, D. B. (1989b). Mode-locked fiber laser with a fiber phase modulator. *Optics Letters*, 14 (13): 680-682 Jul 1 1989.

Russell, P. S. J.; Liu, W. F. (2000). Acousto-optic superlattice modulation in fiber Bragg gratings. *Journal of the Optical Society of America A-Optics Image Science and Vision*, 17 (8): 1421-1429 Aug 2000.

Russo, N. A.; Duchowicz, R.; Mora, J.; Cruz, J. L.; Andres, M. V. (2002). High-efficiency Q-switched erbium fiber laser using a Bragg grating-based modulator. *Optics Communications*, 210 (3-6): 361-366 Sep 15 2002.

Schaffer, C. B.; Garcia, J. F.; Mazur, E. (2003). Bulk heating of transparent materials using a high-repetition-rate femtosecond laser. *Applied Physics A-Materials Science & Processing*, 76 (3): 351-354 Mar 2003.

Siegman, E. (1986). *Lasers*, University Science, Mill Valley, CA, 1986.

Tuchin, V. V. (1993). Lasers and fiber optics in biomedicine. *Laser Physics*, 3 (4): 767-820 1993.

Vicente, S. G. C.; Gámez, M. A. M.; Kiryanov, A. V.; Barmenkov, Y. O.; Andrés, M. V. (2004). Diode-pumped self-Q-switched erbium-doped all-fibre laser. *Quantum Electronics*, 34 (4): 310-314 Apr 2004.

Villegas, I. L.; Cuadrado-Laborde, C.; Abreu-Afonso, J.; Díez, A.; Cruz, J. L.; Martinez-Gámez, M. A.; Andrés, M. V. (2011a). Mode-locked Yb-doped all-fiber laser based on in-fiber acoustooptic modulation. *Laser Physics Letters*, 8 (3): 227-231 Mar 2011.

Villegas, I. L.; Cuadrado-Laborde, C.; Díez, A.; Cruz, J. L.; Martinez-Gámez, M. A.; Andrés, M. V. (2011b). Yb-doped strictly all-fiber laser actively *Q*-switched by intermodal acousto-optic modulation. *Laser Physics, in press* 2011.

Wada, K.; Fujita, J.; Yamada, J.; Matsuyama, T.; Horinaka, H. (2008). Simple method for estimating shape functions of optical spectra. *Optics Communications*, 281 (3): 368-373 Feb 1 2008.

Yu, C. X.; Haus, H. A.; Ippen, E. P.; Wong, W. S.; Sysoliatin, A. (2000). Gigahertz-repetition-rate mode-locked fiber laser for continuum generation. *Optics Letters*, 25 (19): 1418-1420 Oct 1 2000.

Zadok, A.; Raz, O.; Eyal, A.; Tur, M. (2007). Optically controlled low-distortion delay of GHz-wide radio-frequency signals using slow light in fibers. *IEEE Photonics Technology Letters*, 19 (5-8): 462-464 Mar-Apr 2007.

Zalvidea, D.; Russo, N.A.; Duchowicz, R.; Delgado-Pinar, M.; Díez, A.; Cruz, J. L.; Andrés, M. V. (2005). High-repetition rate acoustic-induced Q-switched all-fiber laser. *Optics Communications*, 244 (1-6): 315-319 Jan 3 2005.
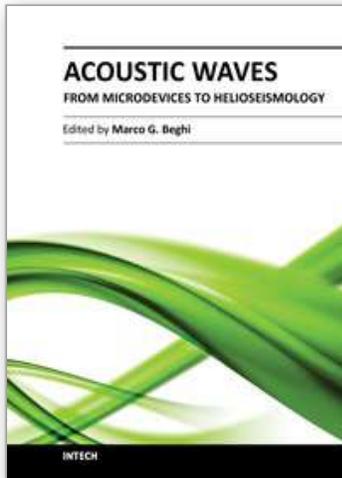
Acoustic Waves - From Microdevices to Helioseismology
Edited by Prof. Marco G. Beghi

The concept of acoustic wave is a pervasive one, which emerges in any type of medium, from solids to plasmas, at length and time scales ranging from sub-micrometric layers in microdevices to seismic waves in the Sun's interior. This book presents several aspects of the active research ongoing in this field. Theoretical efforts are leading to a deeper understanding of phenomena, also in complicated environments like the solar surface boundary. Acoustic waves are a flexible probe to investigate the properties of very different systems, from thin inorganic layers to ripening cheese to biological systems. Acoustic waves are also a tool to manipulate matter, from the delicate evaporation of biomolecules to be analysed, to the phase transitions induced by intense shock waves. And a whole class of widespread microdevices, including filters and sensors, is based on the behaviour of acoustic waves propagating in thin layers. The search for better performances is driving to new materials for these devices, and to more refined tools for their analysis.

How to reference

In order to correctly reference this scholarly work, feel free to copy and paste the following:

INTECH
open science | open minds